PAPER

Check for updates

High-yield synthesis of heavy rare earth(III) anhydrous solvates: known, new, and unexpected products†

Guilherme A. Barbosa, [ID] [a] José Severiano Carneiro Neto, [ID] [a] Bruno J. Stoeberl, [ID] [a] Sarita Wisbeck, [ID] [a] Siddhartha O. K. Giese, [ID] [a] Fabiano Yokaichiya, [b] Daniel da S. Costa, [ID] [b] Andersson Barison, [ID] [a] Ronny R. Ribeiro, [a] Leandro Piovan, [ID] [a] David L. Hughes, [ID] [c] Matteo Briganti, [ID] [d] Giordano Poneti, [ID] [e] Giovana G. Nunes, [ID] [a] Francielli S. Santana [ID] *[a] and Jaísa F. Soares [ID] *[a]

Ten anhydrous rare-earth (RE) chloride solvates were prepared by dehydration of $RECl_3·6H_2O$ with tri-ethylorthoformate (teof) in *O*-donor solvents as an accessible and general synthetic route. Reactions are quick, safe, mild, easily reproducible, and cost-effective. They run at room temperature or under reflux to give high-yield, pure crystalline products that are either new, such as $[Gd_2Cl_4(\mu-Cl)_2(Pr^iOH)_6]$ (**1**) and $[\{GdCl(\mu-Cl)_2(thf)_2\}_\infty]$ (**2**), or obtained for the first time from teof, such as $[GdCl_3(thf)_4]$ (**3**), *trans*-$[MCl_2(thf)_5]trans$-$[MCl_4(thf)_2]$, M = Gd (**4**), Dy (**6**), and Y (**7**), $[YbCl_3(thf)_3]$ (**8**), and $[MCl_3(dme)_2]$, M = Gd (**5**), Dy (**9**), and Er (**10**). Structural and spectroscopic characterization is presented for all products, and variable-temperature magnetic susceptibility data are discussed for the Dy^{3+} complexes **6** and **9**. The latter behaves as a field-induced single-ion magnet for which theoretical (*ab initio*) and experimental data allowed a non-trivial assignment of overlapping high- (Orbach, U_{eff} 139 cm^{-1}) and low-temperature (Raman, w_{eff} 46.8(2) cm^{-1}) magnetic relaxation mechanisms (1 kOe field). Besides the main products, unanticipated Lewis and redox reactivity led to serendipitous **11**, $[\{\{Gd_3Cl_4(\mu-Cl)_4(\mu-H_3CCOO)(C_3H_8O_2)(Pr^iOH)_4\}·Pr^iOH\}_\infty]$, and **12**, $[\{(thf)_2Cl_2Gd(\mu-Cl)_2(\mu_3-O_2)Gd(thf)_3\}_2]·3thf$, whose formation is discussed. The final RE^{3+} anhydrous complexes serve as valuable starting materials for numerous substitution reactions in coordination and organometallic chemistry.

Introduction

Owing to their distinctive electronic and structural properties,[1,2] lanthanoid (Ln^{3+}) complexes have found remarkable applications in medical sciences,[3–7] luminescence,[4,8–11] catalysis,[12–17] magnetism,[18–20] environmental sciences and energy,[14,21–24] among other areas. The ever-growing demand

for improved performances has led to an intensifying quest for simple and rapid preparation routes for Ln^{3+} starting materials, particularly when non-aqueous synthetic methodologies are involved.[25]

While a range of hydrated lanthanoid trihalides and trinitrates are commercially obtainable, their anhydrous equivalents can be costly and not readily available. If, at first sight, preparing anhydrous halides from different Ln sources (metals, oxides, or hydrated salts) seems to be a simple task, several reported methods involve one or more weaknesses, such as high temperature, hazardous chemicals, multiple products, and time-consuming purification steps, resulting in relatively low yields or low cost/benefit. Additionally, commercial anhydrous Ln halides are poorly soluble in organic solvents, limiting their use as reaction precursors.

An early method for preparing anhydrous rare-earth (RE) halides comprises the direct reaction of the metal or the trioxide (RE_2O_3) with the corresponding halogen or hydrogen halide (HX, X = Cl^-, Br^-, I^-) in temperatures above the melting point of the REX_3 products (*ca.* 700 °C).[26,27] Halogenation with

[a]Departamento de Química, Universidade Federal do Paraná, Centro Politécnico, Jardim das Américas, 81530-900 Curitiba-PR, Brazil. E-mail: jaisa.soares@ufpr.br, francielli.s.santana@ufpr.br

[b]Departamento de Física, Universidade Federal do Paraná, Centro Politécnico, Jardim das Américas, 81531-980 Curitiba-PR, Brazil

[c]School of Chemistry, University of East Anglia, Norwich NR4 7TJ, UK

[d]Dipartimento di Chimica "Ugo Schiff", Università degli Studi di Firenze, Via della Lastruccia 3-13, 50019 Sesto Fiorentino, Italy

[e]Dipartimento di Scienze Ecologiche e Biologiche, Università degli Studi della Tuscia, Largo dell'Università, 01100 Viterbo, Italy

†Electronic supplementary information (ESI) available. CCDC 2402796–2402807 and 2403176. For ESI and crystallographic data in CIF or other electronic format see DOI: https://doi.org/10.1039/d5dt00254k

mercury dihalides (HgX_2) is also reported as a high-temperature solid-state reaction.[25,28] Excess reactants and metallic mercury are separated by Hg distillation and REX_3 sublimation, procedures inaccessible for most synthetic laboratories. This method has been improved to prepare $RECl_3$ by standard solution synthesis.[29] Excess of ammonium halides (NH_4X) heated with the trioxides at high temperatures,[30–33] or the oxides being dissolved in acid (HX) in the presence of the ammonium halide[26,34] are nowadays routine approaches for preparing anhydrous RE chlorides and bromides. Other works mention the simple dissolution of the oxide in HX, followed by boiling the resulting solution to dryness, but monohydrate salts are reported to contaminate products.[35] Chlorination of trioxides by carbon tetrachloride or phosgene is also reported, the latter being extremely poisonous, and both methods requiring temperatures of 500–650 °C.[36]

Another procedure allows $LnCl_3 \cdot 6H_2O$ (Ln = Tb, Dy and Nd) to react with organoaluminium compounds such as Bu^i_3Al, Et_3Al, Et_2AlCl, and $EtAlCl_2$ in tri-*tert*-butyl phosphate, $(BuO)_3PO$, giving the corresponding anhydrous $[LnCl_3\{OP(BuO)_3\}_3]$.[37] The drawbacks are the high reactivity of Al alkyls, the specificity of the solvent, and the production of gaseous HCl. Partial dehydration of Gd^{3+}, Er^{3+}, and Y^{3+} salts by sodium hydroxide has also been employed, but the control over the reaction was difficult, leading to polymorphic hexanuclear lanthanoid complexes.[38]

Dehydration by thionyl chloride, in turn, has been one of the most widely applied methods for arriving at anhydrous chlorides, either by heating trioxides under gaseous $SOCl_2$ or by refluxing with the hydrated Ln chlorides under relatively mild conditions.[26,39] The latter requires completion times varying from one up to 110 hours, increasing with the increasing Lewis acidity of the RE ion.[25,35] Both pathways require additional work-up steps for completely removing excess $SOCl_2$ and the toxic reaction byproducts, HCl and SO_2.[39–41]

Because RE cations are well-known hard Lewis acids and thus exhibit good affinity for *O*- or *N*-donor ligands,[42] one way for overcoming solubility problems with anhydrous RE salts consists of preparing solvated halide adducts, especially with coordinating ethers such as tetrahydrofuran (thf) and 1,2-dimethoxyethane (dme).[43] Solvates can be obtained *via* much milder routes than those leading to the "bare" anhydrous halides. Also, they usually show fair solubility in organic media and can be employed in thermodynamically-driven salt elimination reactions.[35] In this context, the (already mentioned) halogenation of RE oxides by mercury dihalides in organic media[44] was one of the earliest reported methods to yield solvates. Silyl halides such as $(CH_3)_3SiX$, $(CH_3)_2SiHX$, and $SiCl_4$ also produce dehydrated RE solvates in reasonable yields from different solvents.[45,46] Less common options employ C_2Cl_6, $C_2H_4X_2$, C_2H_5X, and CH_2X_2 (X = Cl, Br), in which case the metallic RE is sonicated in a solution of the organic halide in the coordinating solvent.[47–49] These preparations are simple and high yield; however, the toxicity and environmental hazards of some of the alkyl halides are drawbacks. Lanthanoid halide solvates have also been obtained by (i) com-

bining the Ln_2O_3/HX/NH_4X protocol with recrystallization in *O*-donor solvents,[34,50–52] (ii) direct reaction of Ln metals with iodine in alcohol and ethers,[53–55] or (iii) carrying out dehydration reactions of $LnX_3 \cdot nH_2O$ in dry coordinating solvents.

Despite the long reaction times, dehydration with thionyl chloride has been widely employed for preparing solvates with reasonable yields.[43,56] Alkyl orthoformates ($HC(OR)_3$; R = Me, Et), in turn, are very handy dehydrating alternatives because of their quick reactions at room temperature, high reactivity, easy handling, and commercial availability. Furthermore, their partial hydrolysis byproducts are alcohols and esters easily removable by distillation or vacuum drying (Scheme S1†), not requiring extensive post-synthesis purification. From this standpoint, using alkyl orthoformates is aligned with green chemistry principles.[57]

While orthoformates are widely applied in organic and d-block chemistry,[58–61] literature comprising their use as dehydration agents in RE chemistry is not extensive. This approach was first adopted to produce $LnCl_3 \cdot nROH$ (R = Me, Et, ^iPr; Ln = La^{3+}, Nd^{3+}, Sm^{3+}, Gd^{3+}, Dy^{3+}, Er^{3+}, Yb^{3+}, and Y^{3+}) by direct reaction of hydrated Ln chlorides with trimethyl orthoformate ($HC(OMe)_3$, tmof) and triethyl orthoformate (teof).[62] Product formulation was based on complexometry, potentiometry, ^1H-NMR spectroscopy, and powder X-ray diffraction analysis, but structural characterization by single-crystal XRD was not presented. The resulting alcohol adducts were subsequently employed as starting materials for *trans*-solvation with triethylamine and acetonitrile.[62] $HC(OMe)_3$ was also used to prepare anhydrous nitrate complexes, $[Ln(NO_3)_3(thf)_3]$ (Y^{3+}, Pr^{3+}, Sm^{3+}, Lu^{3+}) and $[Ln(NO_3)_3(dme)_2]$ (Pr^{3+} and Ho^{3+}), the characterization of which includes X-ray structure resolution.[63]

On the other hand, the hydrolysis of triethyl orthoformate, $HC(OEt)_3$, has scarcely been employed with hydrated Ln ions despite producing less toxic ethanol as the alcohol product (Scheme S1†). Besides the original article by Merbach and co-workers in 1972,[62] the only other report involving teof and lanthanoid(III) complexes describes the *in situ* dehydration of nitrates in the presence of *meso*-1,3-bis(ethylsulfinyl)propane (L) to give crystalline $[\{LnL_2(NO_3)_3\}_n]$ (Ln = La, $n = 1$; Ln = Gd, Dy and Yb, $n = 2$).[64] There are no analogous reactions for RE halides.

Based on the demand for RE starting materials, the present work describes a facile and highly accessible synthetic route to solvated Y^{3+} and late Ln^{3+} precursors in which dehydration with teof is a simple and unifying reaction step. Hydrated lanthanoid chlorides were employed as precursors because halides are better leaving groups for ligand substitution in organic solvents than nitrates. Gadolinium(III) was chosen for several of these syntheses because of its central position in the 4f series; smaller RE^{3+} ions have been included for insight into structural trends. This allows the prediction of similar results with other lanthanoids and illustrates ionic radii effects. In doing so, we revisit earlier literature reports and extend known dehydration routes to highlight triethylorthoformate (teof) as a very convenient synthetic aid, generating products with protic and non-protic coordinating solvents as ligands.

Results and discussion

Overview

The accessible synthetic procedures described in this work allowed the preparation of ten anhydrous, crystalline complexes of the late lanthanoid Gd^{3+}, Dy^{3+}, Er^{3+}, Yb^{3+}, and rare-earth Y^{3+} ions (products **1–10**) in high purity and good yields, with *O*-donor solvents and chloride as ligands. These results illustrate the usefulness of triethylorthoformate in RE dehydration reactions.

Structural and spectroscopic characterizations are presented for all products, starting from those containing Gd^{3+} (complexes **1–5**). Magnetic susceptibility measurements were performed for the Dy^{3+} complexes **6** and **9**, revealing that **9**, $[DyCl_3(dme)_2]$, with dme = dimethoxyethane, is a field-induced single-molecule magnet (SMM) with a highly axial ground doublet. Addressing the relaxation dynamics of **9** by a complementary computational (*ab initio*) and experimental approach led to a precise distinction between Orbach and Raman relaxation mechanisms in overlapping temperature ranges.

Finally, we describe the unexpected decarbonylation and (auto)oxidation that led to two polynuclear Gd^{3+} products, **11** and **12**. Besides exemplifying the reactivity of these Ln^{3+} systems, reporting these results may help interpret some past and future findings of other research groups.

The single-crystal X-ray structures of the new products **1**, **2**, **11**, and **12** are detailed below. Products **3–5** (with Gd^{3+}) and **6–10** (with Dy^{3+}, Y^{3+}, Yb^{3+}, and Er^{3+}), on the other hand, despite being isolated earlier from other preparation routes,[25,35] were also submitted to SC-XRD analysis in this work to confirm their identities because their first synthesis from teof is reported here. These structural data, which compare well with those published in the literature, are presented as ESI (Fig. S2 and S3 and Tables S4–S9†). Powder XRD (Fig. S5 and S6†) and infrared spectroscopy data (Fig. S7–S11†) for all products are also provided as ESI.†

Gadolinium(III) complexes

Scheme 1 shows that dehydration reactions involving Gd^{3+} are remarkably versatile, producing complexes with variable ligands/nuclearities upon changing solvents, temperature, and crystallization conditions. Dehydration in the presence of isopropanol (Pr^iOH) produced binuclear **1**, $[Gd_2Cl_4(\mu\text{-}Cl)_2(thf)_2\}_\infty]$ (**2**), $[GdCl_3(thf)_4]$ (**3**), and *trans*-$[GdCl_2(thf)_5]$*trans*-$[GdCl_4(thf)_2]$ (**4**). In 1,2-dimethoxyethane (dme), mononuclear $[GdCl_3(dme)_2]$ (**5**) is obtained. The highly adaptable structural arrangements involving the "$GdCl_3$" unit align with the minimal stereochemical preferences and small energy differences among coordination geometries for lanthanoid ions.[65] Despite this variability, selecting the coordinating solvent and the reaction conditions (see Experimental) directs the product to the desired species.

The bound tetrahydrofuran molecules are easily lost from the crystalline products **2–4** under vacuum, leaving opaque crystal faces or powdery material depending on crystallite size. This loss, reported for other thf adducts,[66] affects the elemental analysis results. On the other hand, being mostly superficial, it does not prevent structural characterization or purity assessment by single-crystal (SC-XRD) or powder X-ray diffraction (PXRD). Notably, the thf products are hygroscopic and require moisture-free handling, a feature previously reported for anhydrous Ln^{3+} solvates prepared by dehydration with tmof.[62]

The crystals of $[Gd_2Cl_4(\mu\text{-}Cl)_2(Pr^iOH)_6]$ (**1**) and $[GdCl_3(dme)_2]$ (**5**) are more resistant to vacuum drying than the thf solvates, resulting in easier handling. The formation of the dme product **5** from the anhydrous isopropanol complex **1** (Scheme 1) is probably favored by the chelate effect on coordination with dimethoxyethane.

Product **1** is a potential starting material for alkoxide complexes upon deprotonation. Also, its high solubility at room temperature in donor solvents such as ethers (thf, dme) leads to *trans*-solvation. Merbach and co-workers pointed out this possibility in 1972[62] and employed triethylamine and acetonitrile to replace the weak EtOH donor in "$MCl_3 \cdot 3EtOH$", M = early lanthanoids such as La, Pr, and Nd. More recently, Clark and co-workers reported the facile substitution of isopropanol ligands in $[NdI_3(Pr^iOH)_4]$ by thf for the subsequent synthesis of a bis-cyclopentadienyl derivative of neodymium.[67] In the present work, **1** was an effective precursor for synthesizing mononuclear **3** and **5** upon dissolution in thf and dme, respectively (Scheme 1 and Experimental).

SC-XRD analysis of complex 1, $[Gd_2Cl_4(\mu\text{-}Cl)_2(Pr^iOH)_6]$

In the crystals of this binuclear complex, the seven-coordinate Gd^{3+} centers are connected by two chlorido bridges, as seen in Fig. 1. Three Pr^iOH molecules and two terminal Cl^- anions complete the coordination sphere of each metal ion. In the dimeric molecules, the non-bonding Gd···Gd distance is 4.3362(6) Å, while the individual Gd–(μ-Cl) bond lengths differ only slightly from the mean value of 2.7666(8) Å. Average bond distances to the bridging Cl^- are longer than those to terminal ones (2.7666(8) *vs.* 2.6582(8) Å), as expected based on the shared electron density from the chlorido ligands. Crystallographic data and selected structural parameters for **1** are listed in Tables S1 and S2.†

The ligand arrangement around each Gd^{3+} ion in **1** imposes a capped octahedral geometry to each dimer-forming unit, as shown in Fig. 1b and Tables S2 and S14,† with O(1) and O(13) as the capping donor atoms. The Gd–$O_{isopropanol}$ distances do not vary significantly among themselves (values between 2.3695(12) Å and 2.4064(12) Å). These Gd–O bond lengths are within the range of 2.36 to 2.44 Å reported for other Gd^{3+} complexes with similar coordination environments such as $[Gd_4Cl_5(CH_3OH)_{12}(OH)_2]Cl_4 \cdot 3CH_3OH$[68] and $[\{GdFe(OPr^i)_6\}_2(Pr^iOH)]$.[69]

Complex **1** presents one moderate-strength intramolecular hydrogen bond (2.58(3) Å, 166(3)°) involving the O9–H9O bond on Gd1 and the Cl5 atom on Gd2, which imposes the non-planar arrangement adopted by the Gd–(μ-Cl)$_2$–Gd ring
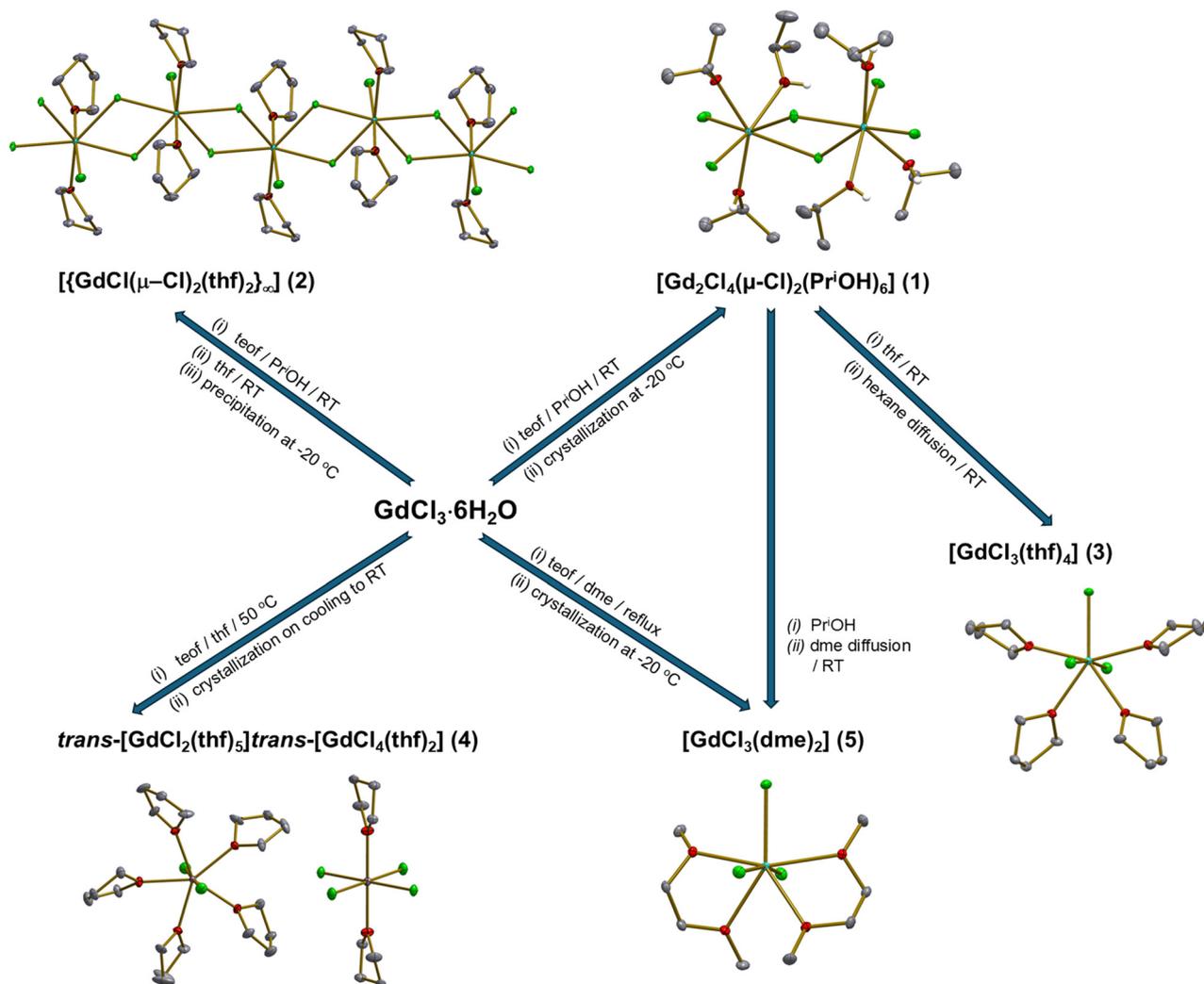
Scheme 1 Synthetic routes employed in this work to prepare anhydrous complexes of Gd^{3+} with isopropanol (Pr^{i}OH), tetrahydrofuran (thf), or dimethoxyethane (dme) as ligands. RT = room temperature and teof = triethylorthoformate.

(Fig. 1a and S2†). Interestingly, in analogous complexes of the larger La^{3+},[70] Ce^{3+},[71] Pr^{3+}[72] or Nd^{3+} ions,[73] the ligand arrangement and the M⋯M distances prevent the occurrence of such interaction. This intramolecular contact and additional intermolecular H bonds of similar strength (involving other isopropanol molecules and chlorido ligands) define the one-dimensional network growing along the crystallographic c axis, alternating the orientation of the Gd–(μ-Cl)$_2$–Gd moieties (Fig. S2†).

In **1**, the paired $\alpha 1/\alpha 2$, $\beta 1/\beta 2$ bond angles defining the Gd1–(μ-Cl)$_2$–Gd2 ring (Scheme 2) are different from each other (Table 1), while they are equal (in each pair) for the larger (and symmetry-related) Ln^{3+} ions mentioned above. This distinction seems to be forced by the O9–H9O⋯Cl5 intramolecular hydrogen bond, which distorts the structural framework. Also, the much smaller Ln⋯Ln distance in the gadolinium dimer, compared to those generated by the early lanthanoid analogs (Table 1), contributes to the Gd$_2$Cl$_2$ ring becoming "squarer" as the average α and β angles get closer.

SC-XRD analysis of complex 2, [{GdCl(μ-Cl)$_2$(thf)$_2$}$_\infty$]

Product **2** is a one-dimensional coordination polymer with GdCl(μ-Cl)$_2$(thf)$_2$ units connected parallel to the b axis by two additional bridging chlorido ligands. For each Gd^{3+} center, one thf and one terminal Cl$^-$ ligands alternate themselves above and below the plane defined by the Gd$_2$Cl$_2$ rings in the chain, while the oxygen atom of the second thf molecule places itself only 0.178(1) Å away from this plane (Fig. 2). Bond angles and ligand arrangement (Table S3†) provide a pentagonal bipyramidal geometry (Table S14†) about the gadolinium ions, in which the smallest bond angle in the equatorial region, (μ-Cl)–Gd–(μ-Cl), is 71.94(3)° (average of two values), while the apical O1–Gd–Cl3 angle is 174.40(3)°.

The Gd–Cl distances in the asymmetrically bridged Gd–(μ-Cl)$_2$–Gd moiety differ *ca.* 0.05 Å from one another. Analogous polymers containing cerium(III),[48,74] praseodymium(III),[48] neodymium(III),[74,75] and yttrium(III)[76] show similar Ln$_2$Cl$_2$ ring dis-
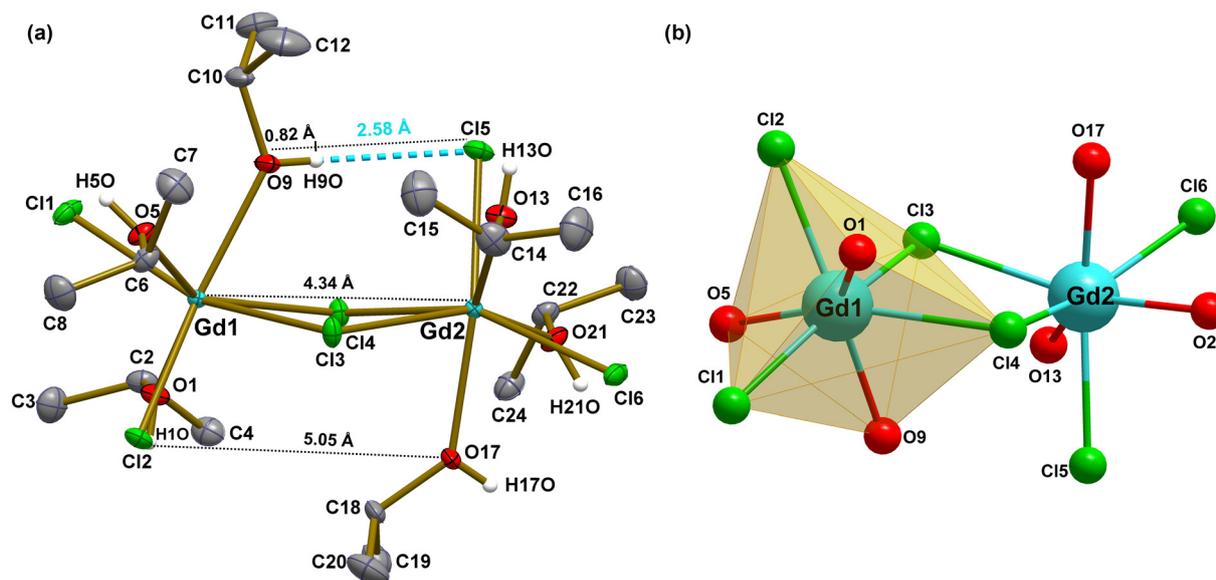
Fig. 1 (a) Representation of the molecular structure of product **1**, with the atom numbering scheme, highlighting an intramolecular hydrogen bond (blue-dashed line) and selected Ln⋯Ln and Cl⋯O contacts (see text). Hydrogen atoms were omitted for clarity, except those forming hydroxyl groups. Thermal ellipsoids were drawn at 50% probability. (b) View of the capped octahedral geometry of each metal center.
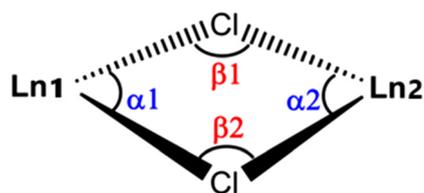
Scheme 2 Schematic representation of the $\alpha 1$, $\alpha 2$, $\beta 1$, and $\beta 2$ angles in binuclear [Ln$_2$Cl$_4$(μ-Cl)$_2$(Pr^{i}OH)$_6$] compounds.

tortions. The absence of strong or medium-strength intra- or inter-molecular interactions is another distinguishing feature of **2**, being compatible with the non-protic nature of the coordinating solvent molecules. Interestingly, there are no reports of analogous coordination polymers featuring the late lanthanoids (from Tb onwards) or even those containing Sm^{3+} or Eu^{3+}. Moreover, with the larger La^{3+} cation, all three chlorides are bridging,[48] (once more) illustrating the versatile coordination abilities of the 4f cations.

Interestingly, Gd^{3+} products **2** (polymeric) and **3**, [GdCl$_3$(thf)$_4$], contain the same ligands and were prepared in similar conditions after dehydration in isopropanol (or from the pre-formed Pr^{i}OH adduct **1**), Scheme 1. These syntheses

differ mainly in the precipitation/crystallization conditions, −20 °C from pure thf for **2** or room temperature after hexane diffusion into the (thf) mother liquor for **3**. A similar occurrence was reported earlier by Sobota et al.,[76] in which the ion pair [YCl$_2$(thf)$_5$]$^+$[YCl$_4$(thf)$_2$]$^-$ produced the polymeric [{YCl(μ-Cl)$_2$(thf)$_2$}$_\infty$] upon solubilization in dichloromethane followed by evaporation to dryness and recrystallization in thf. This shows how subtle complex stabilization is and how probable structural interconversions are when weak field, suitable leaving ligands define the coordination sphere of these versatile cations.

As already mentioned, broad structural flexibility is reported for LnCl$_3$(thf)$_n$ complexes in the solid state, and the favoring of one spatial arrangement to the detriment of another usually correlates the coordination number and nuclearity of the product with the Ln^{3+} ionic radius.[74] Indeed, mononuclear compounds of general formula [LnCl$_3$(thf)$_3$] (Ln = Yb and Lu) and [LnCl$_3$(thf)$_4$] (Ln = Nd, Sm, and Gd), for example, have been obtained for late and early lanthanoid(III) ions respectively, and the increasing coordination number on moving left in the series illustrates the effect of the larger ionic radii.[56,77] Accordingly, coordination polymers such as [{La(μ-Cl)$_3$(thf)$_2$}$_\infty$] and [{LnCl(μ-Cl)$_2$(thf)$_2$}$_\infty$] (Ln = Ce, Pr, and Nd)

Table 1 Bond angles ($\alpha 1$, $\alpha 2$, $\beta 1$ and $\beta 2$, degrees) and Ln⋯Ln distances (Å) in the Ln$_2$Cl$_2$ rings of the binuclear complexes [Ln$_2$Cl$_4$(μ-Cl)$_2$(Pr^{i}OH)$_6$]

Ln^{3+}	$\alpha 1$	$\alpha 2$	$\beta 1$	$\beta 2$	Ln⋯Ln	Temperature/K	Ref.
La	71.96(2)	71.96(2)	108.04(2)	108.04(2)	4.785(1)	295	70
Ce	72.09(9)	72.09(9)	107.91(9)	107.91(9)	4.719(2)	153	71
Pr	71.96(2)	71.96(2)	108.04(2)	108.04(2)	4.6803(4)	150	72
Nd	72.08(4)	72.08(4)	107.92(5)	107.92(5)	4.646(2)	295	73
Gd	75.214(14)	75.692(14)	103.923(15)	102.485(15)	4.3362(6)	100(2)	This work
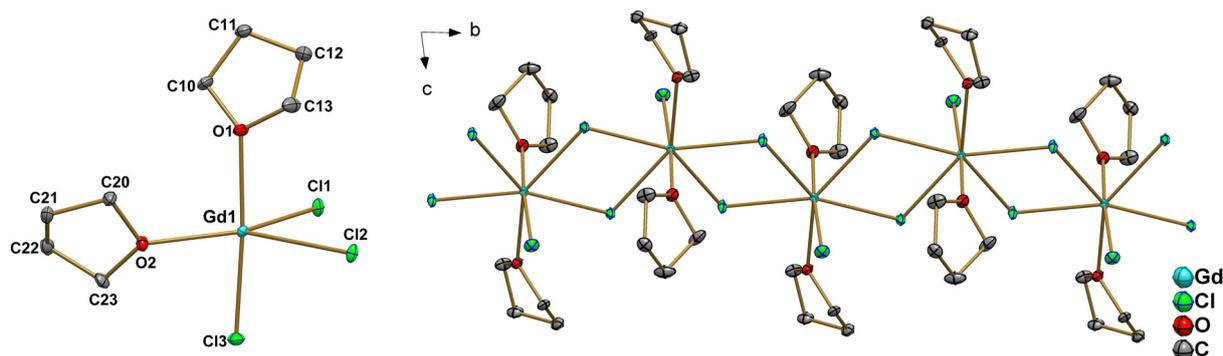
Fig. 2 Left: View of the asymmetric unit of [{GdCl(μ-Cl)$_2$(thf)$_2$}$_\infty$] (product **2**) with the atom numbering scheme. The hydrogen atoms were omitted for clarity. Right: Representation of the coordination polymer chain growing along the *b*-axis in the unit cell. Thermal ellipsoids were drawn at 50% probability.

are formed preferably with early 4f ions, where the aggregation is driven by electron deficiency and large spatial requirements.[48] In this case, the isolation of [{GdCl(μ-Cl)$_2$(thf)$_2$}$_\infty$] in this work, but not of the Dy^{3+} analog (see below), suggests that this particular pattern of polynuclear aggregation encounters its limit in the middle of the 4f series.

Dehydration reactions of RECl$_3$·6H$_2$O (RE = Y^{3+} and late lanthanoids) with teof in tetrahydrofuran and dimethoxyethane

While Gd^{3+} chloride in thf is versatile in producing both molecular (**2** and **3**) and discrete ion pair (**4**) complexes, the smaller Dy^{3+} and Y^{3+} cations (effective ionic radii for 6-coordination 91.2 and 90.0 pm, respectively)[78] gave only the *trans*-[RECl$_2$(thf)$_5$]*trans*-[RECl$_4$(thf)$_2$] compounds **6** and **7** (Scheme 3). Interestingly, the even smaller Yb^{3+} (effective ionic radius 86.8 pm)[78] produced only the molecular, mononuclear complex **8** but with three coordinated thf molecules instead of the four seen in [GdCl$_3$(thf)$_4$]. This again illustrates ionic radii constraints. Single-crystal X-ray diffraction characterization of the products is presented as ESI (Fig. S3 and S4; Tables S4–S9†).

The formation of the ion pair products **4**, **6**, and **7** has been assigned to the autoionization of the rare-earth chloride in the presence of the polar solvent (eqn (1)):[75]

$$2 \ RECl_3(thf)_{3.5} \ \rightleftharpoons \ [RECl_2(thf)_5]^+[RECl_4(thf)_2]^- \qquad (1)$$
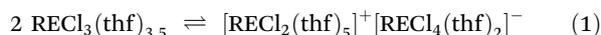
This proposal is compatible with the high dielectric constant of thf (7.6).[79] Temperature seems to play a role since [GdCl$_2$(thf)$_5$][GdCl$_4$(thf)$_2$] (**4**) was obtained after heating at 50 °C while [GdCl$_3$(thf)$_4$] (**3**) was prepared at room temperature. Consistently, the literature mentions the autoionization of "DyCl$_3$(thf)$_{3.5}$" to give the dysprosium(III) analog of **4** upon heating the reaction mixture under reflux.[75] In the present work, increasing the temperature was also necessary to prepare the isostructural Dy^{3+} and Y^{3+} complexes [DyCl$_2$(thf)$_5$][DyCl$_4$(thf)$_2$] (**6**) and [YCl$_2$(thf)$_5$][YCl$_4$(thf)$_2$] (**7**) (see Experimental).

Solvates **3**,[56] **4**,[48] **6**,[75] **7**,[76] and **8**[48] were described earlier after dehydration of Ln chlorides with thionyl chloride (**3**, **6**), direct reaction of the lanthanoid metal with hexachloroethane

in tetrahydrofuran (**4**, **8**), or direct reaction of anhydrous YCl$_3$ with thf under reflux (**7**). Their solubility in tetrahydrofuran and small-chain alcohols indicates their usefulness as starting materials in subsequent reactions.

Expanding the range of *O*-donor ligands, the dehydration procedure with teof also allowed isolating, in the present work, three isostructural [LnCl$_3$(dme)$_2$] complexes, Ln = Gd (**5**), Dy (**9**), and Er (**10**) (Fig. S3†), whose synthesis had already been reported but from the treatment of Ln$_2$O$_3$, Ln$_2$(CO$_3$)$_2$, or LnCl$_3$·nH$_2$O with thionyl chloride, or from [Dy$_2$Cl$_6$(thf)$_7$] in boiling dme.[35,49,80,81] The effect of decreasing ionic radii from Gd to Er manifests itself clearly in the bond distances and angles (Tables S6 and S7†). The advantages of the present route reside in mild reaction conditions, easy and safe handling of teof, quick synthetic procedure, and high isolation yields.

Magnetic susceptibility measurements for the Dy^{3+} complexes 6 and 9

Dysprosium(III) complexes, featuring high spin (S = 5/2) and orbital (L = 5) quantum numbers, show relatively high uniaxial magnetic anisotropy that makes them ideal candidates for Single Ion Magnets (SIM), *i.e.*, zero-dimensional magnetic systems with slow-relaxing magnetization.[82,83] For lanthanoid-based molecular nanomagnets, magnetization dynamics can be tuned by coordination geometries and ligand field strength and orientation,[84,85] bipyramidal pentagonal (maximum symmetry D_{5h}) being one of the promising coordination spheres to reduce quantum tunneling and thus increase the magnetic relaxation times.[86,87] This prompted us to investigate the magnetic susceptibilities of the two Dy^{3+} complexes prepared in this work, *trans*-[DyCl$_2$(thf)$_5$]*trans*-[DyCl$_4$(thf)$_2$] (**6**) and [DyCl$_3$(dme)$_2$] (**9**). For product **6**, the magnitude of $\chi_M T$ measured at room temperature (300 K) equals 27.7 emu K mol^{-1}, as seen in Fig. S12-left,† and agrees well with the calculated for two magnetically isolated Dy^{3+} ions (28.3 emu K mol^{-1}), again evidencing the purity of the product. The decrease in $\chi_M T$ with decreasing temperature, starting from 300 K, can come from the depopulation of the crystal-field

trans-[LnCl$_2$(thf)$_5$]*trans*-[LnCl$_4$(thf)$_2$]
Ln = Dy^{3+} (**6**)
Ln = Y^{3+} (**7**)

[LnCl$_3$(thf)$_3$]
Ln = Yb^{3+} (**8**)

(i) teof / thf / 70-80 °C
(ii) crystallization at -20 °C

(i) teof / thf / RT
(ii) crystallization at -20 °C

LnCl$_3$·6H$_2$O

(i) teof / Pr^{i}OH / dme
(ii) crystallization at RT

(i) teof / dme / reflux
(ii) crystallization at -20 °C

[LnCl$_3$(dme)$_2$]
Ln = Dy^{3+} (**9**)

[LnCl$_3$(dme)$_2$]
Ln = Er^{3+} (**10**)
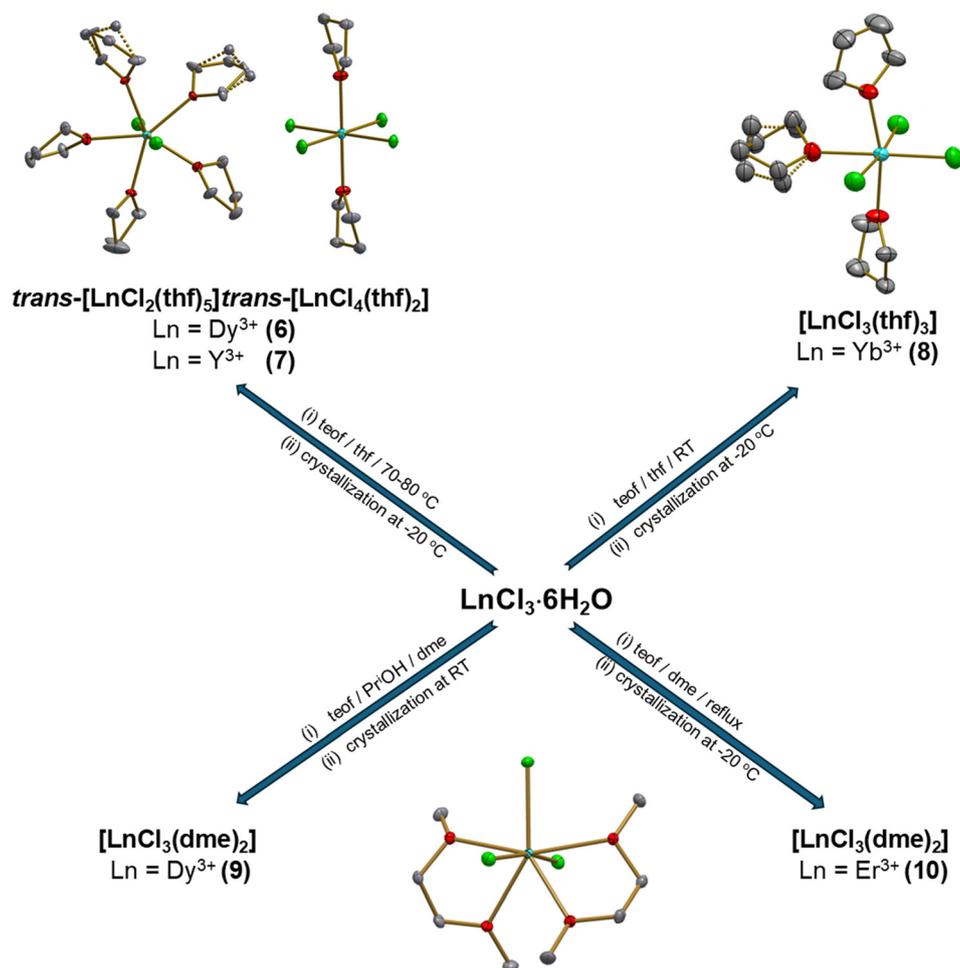
Scheme 3 Synthetic routes to anhydrous thf and dme solvates **6–10**.

split doublets, an antiferromagnetic-type (intermolecular) interaction between the dysprosium(III) ions, or both.

AC susceptibility measurements of **6** revealed a dependence of the in- and out-of-phase magnetic susceptibilities on the temperature (Fig. S13†), but no peaks in the out-of-phase χ_M component with or without an applied static field, evidencing the lack of slow magnetic relaxation and SIM behavior. This probably comes from the weak axial crystal field in both complex ions in **6**, even if a dipolar interaction in the solid state can also account for this behavior. Indeed, in the crystal structure of **6**, the shortest Dy⋯Dy distance is 7.7702(4) Å, comparing well with that in the isostructural product **4** (smallest Gd⋯Gd separation 7.7884(5) Å). For the latter, EPR spectroscopy reveals the broadest solid-state spectra among all Gd^{3+} complexes (Fig. S16†), suggesting the presence of relevant dipolar magnetic interaction. The significance of these distances is exemplified by complex **3**, [GdCl$_3$(thf)$_4$], in which the closest Gd ions in the crystalline state are the farthest apart amongst all gadolinium complexes reported in this work (Gd⋯Gd 8.7303(4) Å). Accordingly, the EPR spectra of **3** at 300 and 77 K are the best resolved (Fig. S16†). It is also possible that the loss of weakly bound thf, particularly upon grinding

the crystals of **6** for sample preparation, affected the measurements by changing the local environment of the Dy ions.

In the case of product **9**, [DyCl$_3$(dme)$_2$], the value of $\chi_M T$ measured at room temperature (13.7 emu K mol^{-1}, Fig. S12-right†) is also in agreement with the calculated for one Dy^{3+} center (14.2 emu K mol^{-1}). *Ab initio* calculations (see Computational details) for **9** showed a first excited state quite high in energy (139 cm^{-1}, Table S16†) and an axial magnetic anisotropy tensor for the ground state (g_z close to 20, Table S17† and Fig. 3). These two features make **9** a good candidate for the observation of slow-relaxation of magnetization of molecular origin.

With no static field applied, no out-of-phase magnetic susceptibility (χ''_M) peaks were observed for **9**, indicating fast relaxation processes, including quantum tunneling. This agrees with the computational results, which showed sizeable transverse g-factors in the ground state (Table S17†). In this case, however, the situation changed after applying a field of 1 kOe, and two sets of χ''_M peaks shifting with temperature were observed (Fig. 4-left). The fast-relaxing set, observed in the 1.9–6.0 K interval, produced the relaxation times (τ) shown in the right panel of Fig. 4 (orange circles) after fitting with the
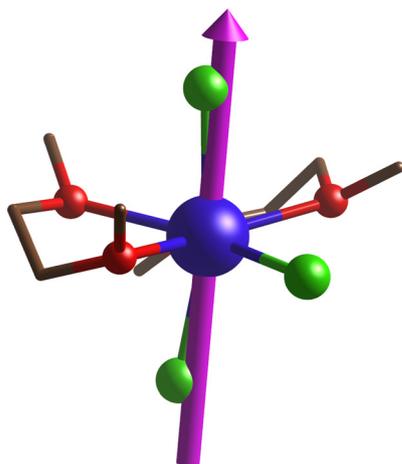
Fig. 3 Orientation of the ground Kramers magnetic easy axis (purple arrow) in the molecular frame for compound **9**. Color code: Dy/blue, Cl/green, O/red, C/brown.

extended Debye model.[88,89] In this case, an Arrhenius-like behavior was observed only above 3.7 K, leading to an effective barrier to the thermally activated magnetic relaxation (U_{eff}) of 51.1 K (36.8 cm^{-1}). Such attribution should be taken carefully because this activation barrier does not match the computed energy spacings between the ground and the excited doublets (Table S16†). In the region between 1.9 and 3.7 K, on the other hand, a decrease in the relaxation time with increasing temperature is observed (Fig. 4-right, orange circles), a phenomenon attributed to a phonon-bottleneck effect – a lack of vibrations necessary to activate magnetic relaxation at low temperatures.[90,91]

The other, lower frequency χ''_M set of peaks yielded the Arrhenius graph presented in Fig. 4-right (black circles), which could be adjusted with a magnetic relaxation model involving two mechanisms, Orbach (Arrhenius) and Raman (eqn (2)), providing the parameters reported in Table S15.† The α values found in the extended Debye model fitting – the parameter that describes the width of the statistical distribution of magnetic relaxation times – range between 0.05 and 0.01 for product **9** (Fig. S15†). This indicates a very narrow distribution and, therefore, a highly similar environment of the relaxing magnetic dipoles in the sample.

$$\tau^{-1} = \tau_{Orbach}^{-1} + \tau_{Raman}^{-1} = \tau_{0,\,Orbach}^{-1} e^{\frac{-U_{eff}}{k_B T}} + \tau_{0,\,Raman}^{-1} \frac{e^{\frac{W_{eff}}{k_B T}}}{\left(e^{\frac{W_{eff}}{k_B T}} - 1\right)^2}$$

(2)

In eqn (2),[92] the first term on the right describes the Orbach mechanism, which requires energy transfer through spin–lattice coupling to overcome the barrier for magnetization reversal (U_{eff}). To reduce overparametrization, this value has been fixed to the one arising from the *ab initio* calculations (139 cm^{-1}, Table S16†). The second term corresponds to the Raman mechanism, which also operates through selective vibrational modes but involves virtual energy states whose energy (w_{eff}) acts as an Arrhenius-like barrier.[92] Attempts to include a direct relaxation process instead of the Orbach or Raman mechanisms led to slightly worse fittings and were discarded. Complementary experimental and computational analyses allowed us to discern between two relaxation regimes for compound **9**: a Raman one, taking over in the lower temperature range, and an Orbach process, overruling the former above 13 K, in line with the presence of higher-energy phonons in this temperature range, capable of triggering the transition between the two lowest Kramers doublets.

Despite the favorable pentagonal-bipyramidal geometry exhibited by the first coordination sphere (Table S14†), the
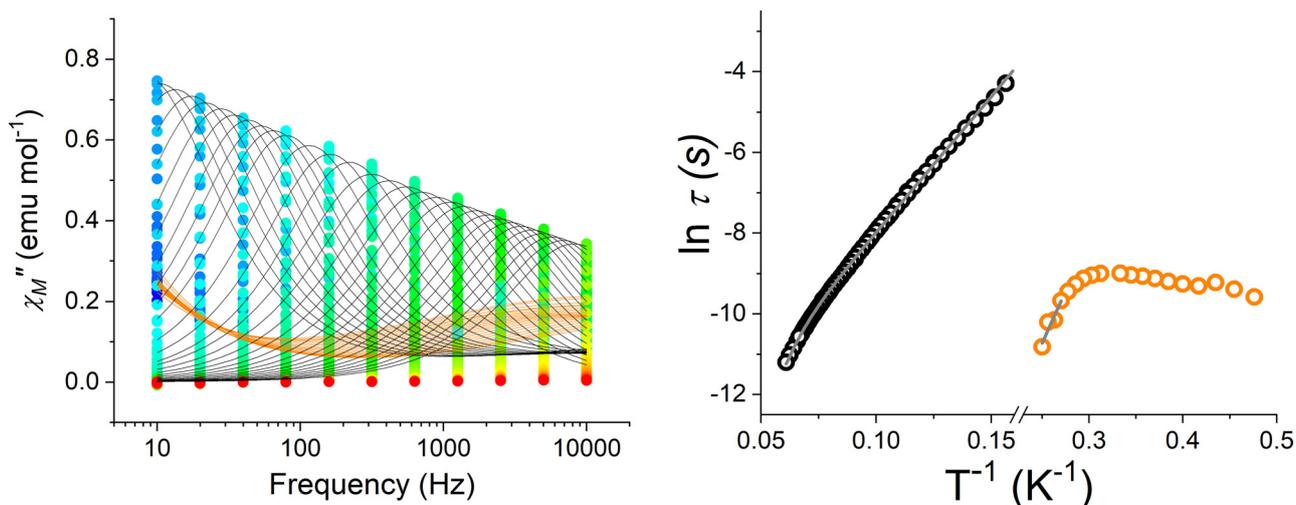
Fig. 4 Left: Dependence of the two $\chi''_M(\nu)$ components with frequency for product **9** in a 1.0 kOe static field. Full lines describe the best fitting functions (orange for the high-frequency process, black for the low-frequency one). Right: Arrhenius plot for the slow (black circles) and fast (orange) relaxation processes, along with best fitting lines, calculated as described in the text. See Table S15† for the full set of best-fitting parameters.

relaxation features of **9** are average. We attribute this behavior to the actual symmetry of the complex, which is significantly lowered from the ideal D_{5h} by the chelating nature of the dme ligands and the presence of different donor atoms bound to Dy^{3+}. This is illustrated (Table S7†) by the small O–Dy–O angles in the five-membered chelate rings (67.51(13)° for O1–Dy–O2 and 66.61(13)° for O3–Dy–O4), the large deviation of O3 and O4 from the average equatorial plane (0.416 and 0.468 Å respectively), and the Cl3–Dy–Cl2 angle far from linearity (168.39(4)°). These geometrical features usually influence several other parameters relevant to the relaxation dynamics in single-ion magnets, the phonon spectrum of the material[93] and the detailed ground and excited doublets compositions[94] being the most relevant ones.

Serendipitous reactions leading to polynuclear Gd^{3+} products 11 and 12

Complex 11, [({Gd_3Cl_4(μ-Cl)_4(μ-H_3CCOO)(C_3H_8O_2) (Pr^iOH)_4}·Pr^iOH)_∞]. An early attempt to run the dehydration reaction that gave complex **1**, [Gd_2Cl_4(μ-Cl)_2(Pr^iOH)_6], employing a large excess of teof in isopropanol, produced the unexpected product **11**, [({Gd_3Cl_4(μ-Cl)_4(μ-H_3CCOO)(C_3H_8O_2) (Pr^iOH)_4}·Pr^iOH)_∞]. The Experimental section and ESI† present details of the synthesis and FTIR characterization (Fig. S7†).

Fig. 5 shows the asymmetric unit, {Gd_3Cl_4(μ-Cl)_4(μ-H_3CCOO)(Pr^iOH)_4(C_3H_8O_2)}·Pr^iOH, of this unprecedented coordination polymer, while Table S10† gathers selected bonds and angles involving the gadolinium cations. The two "external" Gd(1) and Gd(3) centers are each bonded to one terminal chloride, Cl(1) or Cl(7), two isopropanol molecules, three bridging chlorides, and one oxygen atom of the bridging acetate ligand; this sevenfold coordination shows a slightly distorted pentagonal bipyramidal geometry (Table S14†). Gd(2), in turn, is eight-coordinate with two terminal chlorides, Cl(4) and Cl(5), the two oxygen atoms of a bridging acetate ligand and two oxygen donor atoms from a chelating 2-methoxyethanol molecule in a biaugmented trigonal prismatic geometry (Table S14†). The acetate ligand, also adopting a chelating mode, bridges the three Ln^{3+} ions.

Gd(2) is therefore bonded to Gd(1) and Gd(3) via the acetate's O(3) and O(6), respectively, and two chlorido ligands, Cl(3) and Cl(6). The effect of the higher coordination number in Gd(2) manifests itself in the significantly longer bonds to the terminal chlorides, 2.7336(11) and 2.7109(11) Å to Cl(4) and Cl(5) respectively, compared with those involving the seven-coordinate Gd(1) and Gd(3), 2.5615(13) Å to Cl(1) and 2.5596(13) Å to Cl(7). These large Gd–Cl bond distances involving Gd(2) are close to the bridging Gd–(μ-Cl)–Gd bond lengths (ca. 2.75 Å on average), as mentioned below. Also, the acetate's oxygen atoms bind more strongly to Gd(1) and Gd(3) (bridging mode) than to Gd(2) (chelating), with average bond lengths of 2.41 vs. 2.51 Å, respectively.

The one-dimensional polymeric chain grows from these "Gd_3 monomers" by connecting vicinal Gd(1) and Gd(3) through the double Cl(2) and Cl(8) bridges along the crystallo-

graphic a direction (Fig. 6). The shortest non-bonding Gd···Gd distances inside the repeating trinuclear unit are 4.2254(5) Å (Gd1···Gd2) and 4.2299(4) Å (Gd2···Gd3), while the Gd1···Gd3 separations involving neighboring building blocks equal 4.3333(4) Å. Consistent with these similar dimensions, all Gd–(μ-Cl)–Gd bonds are close in length, ranging from 2.7336(11) to 2.7664(12) Å regardless of being located inside or between the repeating Gd_3 units. The linear skeleton of the chain is formed by the recurring (μ-Cl)_2–Gd1–(μ-acetato-O,O')–Gd3–(μ-Cl)_2 motif, with the Gd(2) centers placed above or below this main line as determined by the inversion symmetry of the cell.

The unit cell contains one isopropanol molecule per trinuclear Ln^{3+} unit. These solvating molecules connect the polymer chains by involving in intermolecular, medium-strength H-bonding (HB) to O(4), in the 2-methoxyethan-1-ol ligand, and weak HB to Cl(4) in the parallel chains (dashed blue lines in Fig. 6). Weak, intramolecular hydrogen bonds are also observed between the isopropanol molecules coordinated to Gd(1) and Gd(3) and the terminal chlorido ligands on Gd(2), Fig. 6, helping to shape and stabilize the polynuclear aggregation.

Differently from all the other complexes synthesized in this work, whose structures have precedent in rare-earth chemistry, product **11** is unparalleled, and the observation of both 2-methoxyethanol and acetate bound to Gd(2) draws immediate attention. The Ln-alkoxyalcohol adduct probably results from single dme C–O bond cleavage, resembling the reported reactions between strongly oxophilic MX_5 (M = Nb, Ta; X = Cl, Br) and different 1,2-dialkoxyalkanes in CH_2Cl_2 at room temperature.[95,96] This reactivity of the C–OMe bond in dme has been explored in the acid-catalyzed synthesis of methylethers from alcohols, in which dme is employed as the methylating agent.[97] It is thus possible that the coordination of dme by the Lewis acidic Gd^{3+} ions causes the activation of the O–Me bond, transforming the methyl group in an electrophilic center to be attacked by an ethanol molecule (coproduct of teof hydrolysis). This leads to O–Me bond cleavage, producing the methoxyethanol ligand in **11** and the very volatile methoxyethane.

On the other hand, we have not yet been able to provide a reasonable explanation for the coordination of acetate to the Gd^{3+} center in **11**. Looking at the capture of peroxide derived from O_2 in product **12** (see below), one could hint at a peroxide-containing intermediate in Ln-catalyzed acyl oxidation leading to the acetate-centered assembly of **11**. Although this looks like a long shot, polynuclear rare-earth complexes are reported to catalyze the oxidation of aldehydes to carboxylates[98] by insertion of O_2 from the air into an acyl group, yielding a peroxy acid that rearranges to yield the carboxylic acids.[99] A ketone oxidation during the assembly of a dodecanuclear lanthanum(III) aggregate is also believed to follow a similar pathway.[100]

Looking for possible reactive species, we conducted an extensive ^1H and ^{13}C solution NMR investigation to identify all the volatiles recovered from the reaction mixture that gave **11** (Fig. S17 and S18; Table S13†) and confirm the purity of the commercial teof provided by two different suppliers. We found
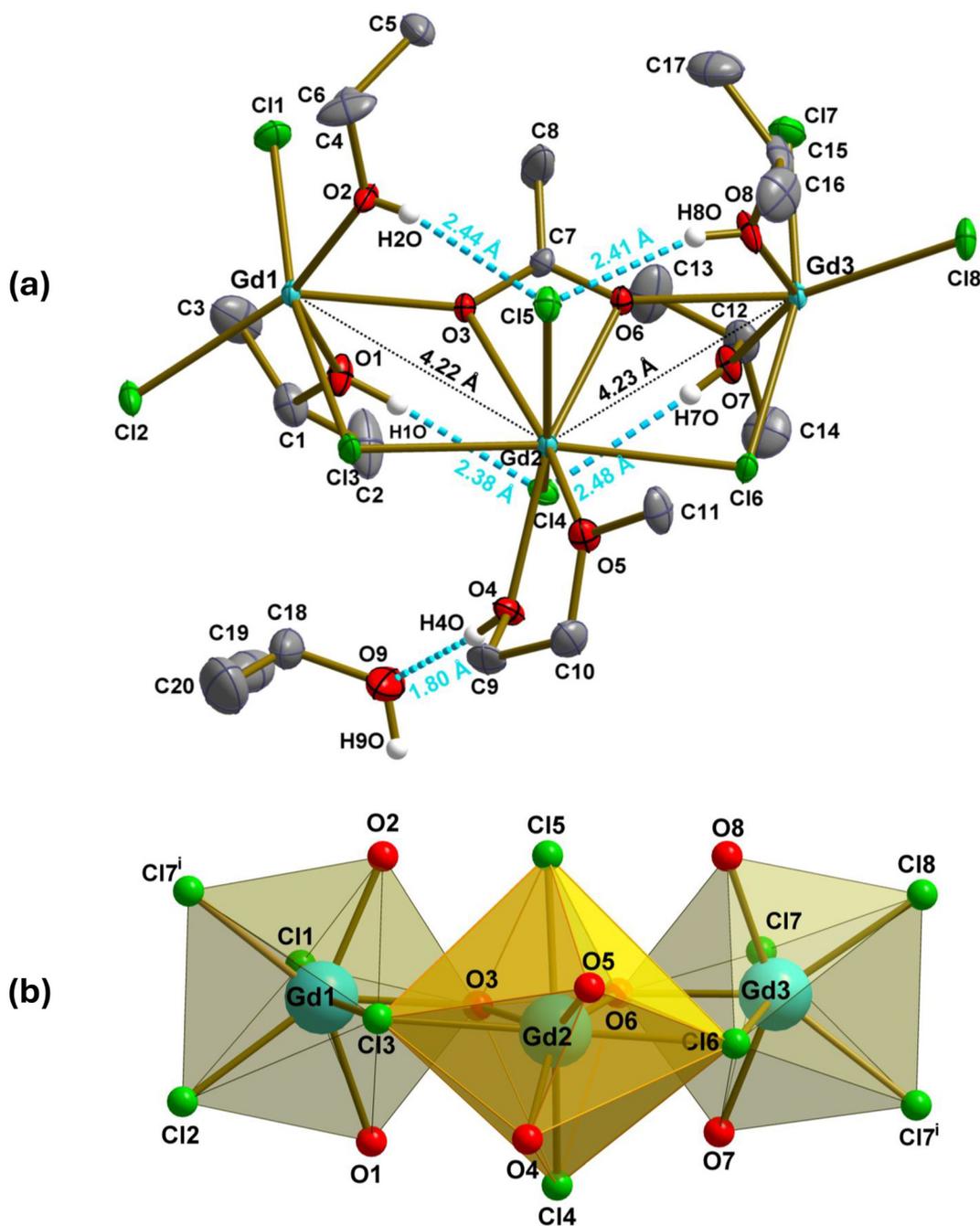
Fig. 5 (a) Representation of the asymmetric unit of product **11** (plus adjoining, bridging chloride ligands), with the atom numbering scheme, highlighting intra and intermolecular hydrogen bonds (blue-dashed lines) and Ln···Ln contacts. Hydrogen atoms were omitted for clarity, except those forming hydroxyl groups. Thermal ellipsoids were drawn at 50% probability. (b) View of the pentagonal bipyramidal (Gd1 and Gd3) and biaugmented trigonal prismatic (Gd2) geometries of the metal centers.

no sign of acetic acid or an obvious source of acetyl functionality apart from the 'hard-to-oxidize' ethanol, which still leaves us with an open question. What we know for sure is that the hydrolysis of the large amount of teof employed in this synthesis, the extensive work-up (see Experimental), and the long stand of the reaction mixture at −20 °C (about one month) after vapor diffusion of dme gave rise to the unexpected

ligands in **11**. This reinforces that orthoesters such as HC(OEt)$_3$ can play several roles in organic synthesis,[57,58] and their hydrolysis in the presence of lanthanoid species, either under N$_2$ or trace amounts of air, expands possibilities beyond the usual products.

Complex 12, [{(thf)$_2$Cl$_2$Gd(μ-Cl)$_2$(μ$_3$-O$_2$)Gd(thf)$_3$}$_2$]·3thf. In one repetition of the synthesis of [{GdCl(μ-Cl)$_2$(thf)$_2$}$_\infty$]
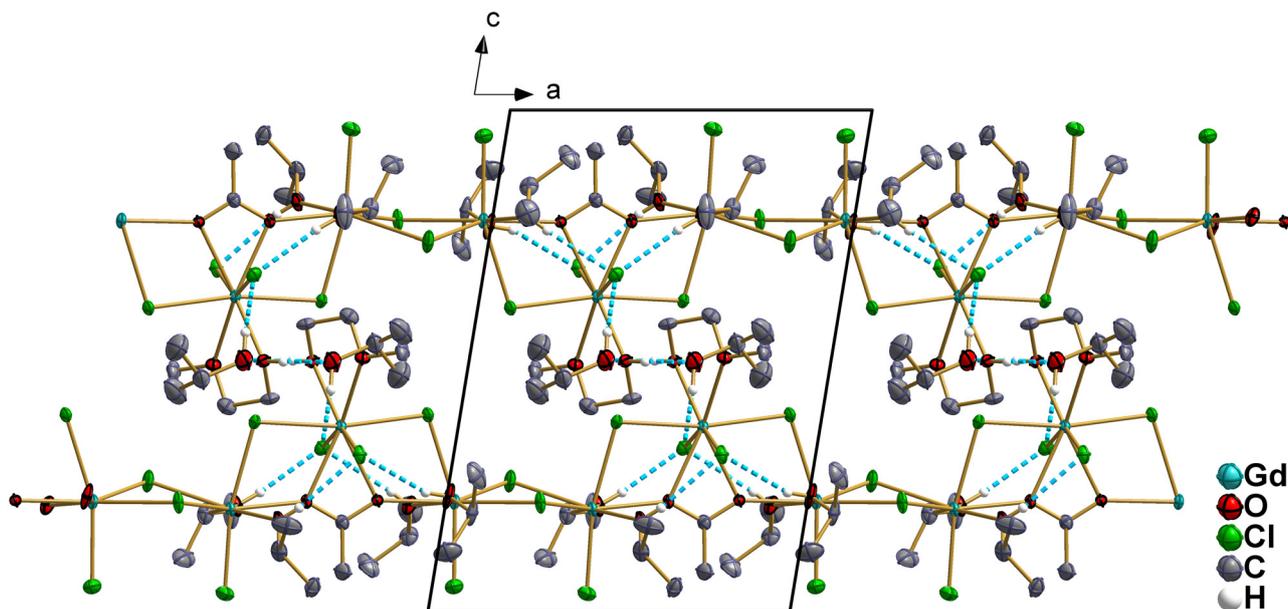
Fig. 6 Representation of the coordination polymer [({Gd$_3$Cl$_4$(μ-Cl)$_4$(μ-H$_3$CCOO)(C$_3$H$_8$O$_2$)(Pr^{i}OH)$_4$}·Pr^{i}OH)$_\infty$] (product **11**) growing along the *a* axis. The hydrogen atoms were omitted for clarity, except those (hydroxyl groups) involved in intra- and inter-molecular hydrogen bonds (dashed blue lines). Thermal ellipsoids were drawn at 50% probability.

(product **2**), after the isolation of the main product, the filtrate was cooled down to −20 °C in an attempt to obtain larger crystals (see Experimental). After two weeks at this temperature, a batch of colorless blocks was filtered off and analyzed by single-crystal X-ray diffractometry to reveal the accidental peroxide-template assembly[98,101] of the tetranuclear product **12**, [{(thf)$_2$Cl$_2$Gd(μ-Cl)$_2$(μ$_3$-O$_2$)Gd(thf)$_3$}$_2$]·3thf (Fig. 7).

The structure of **12** closely resembles those described by Neumüller and colleagues[102] for [Ln$_4$(O$_2$)$_2$Cl$_8$(py)$_{10}$]·py, in which Ln = Sm, Eu, and Gd. These were obtained from [LnCl$_3$(daa)$_2$] (daa = 4-hydroxy-4-methyl-2-pentanone) dissolved in pyridine under reflux and left to stand in the air for several days. That was the first report of the μ$_3$-η^2:η^2:η^2 peroxide coordination mode, and still is the only other description of the rare tetranuclear skeleton found in **12** (Fig. 7 and S4†). Despite this structural similarity to the pyridine adducts, **12** is, in fact, unique, as there is no description of any thf-containing analog with another rare-earth ion.

The centrosymmetric molecule has two types of non-equivalent gadolinium(III) centers. Thus, Gd1 and Gd1^i are bound to two bridging and two terminal chlorido, one η^2-peroxido, and two neutral (thf) ligands. The other two metal ions, Gd2 and Gd2^i in Fig. 7, are connected to both peroxido ligands, two bridging Cl$^-$, and three thf molecules. This tetranuclear core is shown in Fig. S4a,† which emphasizes the nearly octahedral geometry of the central (Gd2)$_2$(O$_2$)$_2$ motif. The packing arrangement (Fig. S4b†) is new compared to Neumüller's report, with **12** crystallizing in the monoclinic instead of the triclinic system (Table S1†) and three solvating thf (instead of one py) molecules per Ln$_4$ unit. The only (inter)molecular contact
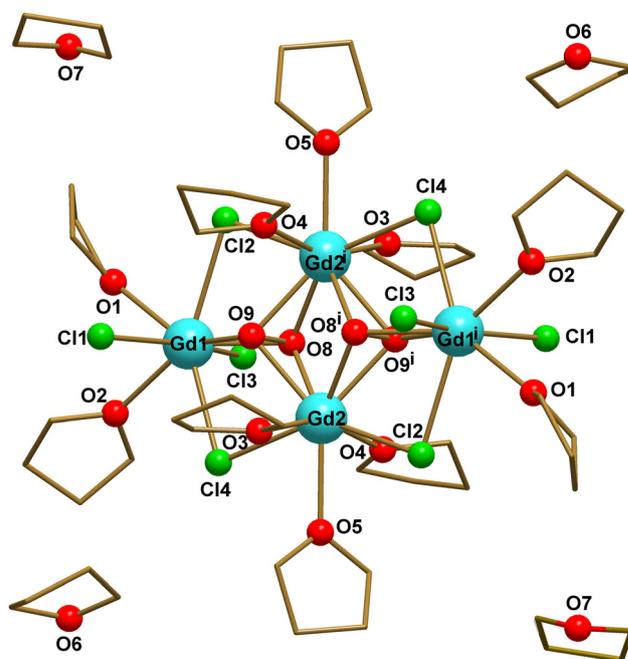
Fig. 7 Molecular structure of complex **12**, [{(thf)$_2$Cl$_2$Gd(μ-Cl)$_2$(μ$_3$-O$_2$)Gd (thf)$_3$}$_2$]·3thf, with the heteroatom numbering scheme. Symmetry code: (i) −x + 1, −y + 1, −z + 1.

involving this non-coordinated solvent is C(24)–H(24A)···Cl(4), connecting a bridging chlorido ligand to a thf molecule. Such weak interaction (Table S12†) does not prevent the quick loss of lattice solvent when the crystals are isolated from the mother liquor at room temperature. Consequently, the product

becomes powdery and loses crystallinity, impairing complete characterization. Weak intramolecular contacts also involve H atoms in coordinated thf molecules and nearby Cl atoms (Table S12†).

The peroxido O8–O9 bond length in **12**, 1.526(3) Å (Table S11†), is well inside the range reported for the very few known Gd-peroxido complexes with the O_2^{2-} ligand in the μ^3-η^2:η^2:η^2 binding mode.[103–106] The peroxido atoms place themselves 0.749(2) (O8) and 0.777(2) Å (O9) above and below the strictly planar eight-membered Gd1–Cl4–Gd2–Cl2^i–Gd1^i–Cl4^i–Gd2^i–Cl2 ring. The non-bonding Gd2⋯Gd2^i, Gd2⋯Gd1, and Gd1⋯Gd2^i distances in each half of the complex equal 3.5680(5), 3.9874(5), and 4.0016(7) Å, respectively, producing two isosceles triangles fused by the central Gd2⋯Gd2^i vector. This differs significantly from the heteronuclear [Gd$_3$Ni$_3$(H$_2$O)$_3$(mpko)$_9$(O$_2$)(NO$_3$)$_3$]·NO$_3$ (Hmpko = 1-(pyrazin-2-yl)ethanone oxime) and [Gd$_3$Zn$_3$(O$_2$)L$_3$(PyCO$_2$)$_3$](OH)$_2$(ClO$_4$)$_2$ (H$_2$L = *N,N′*-bis(3-methoxysalicylidene)-1,3-diaminopropane), also containing triply-bridging η^2:η^2:η^2 peroxido ligands, where the triangular Gd$_3$ units are equilateral with a C_3 rotational axis coinciding with the O–O bond.[103,105]

The structure shows disorder about a special position for one of the crystallizing thf molecules (O7, C24–C28). In this case, there is an inversion center in the middle of the thf ring; therefore, although none of the five atoms lies in the special position, on average, the whole molecule is disordered about the inversion center. In the refinement, the occupancy factor for the five atoms was set to 0.5.

Like other examples of Ln-peroxide complexes described in the literature,[98,106,107] the formation and incorporation of O_2^{2-} in **12** is ascribed to the reduction of molecular oxygen from the air and the highly oxophilic character of the lanthanoid ions. Incidental O_2 probably came in contact with the reaction mixture during or after the isolation of product **2** (see Experimental), and the subsequent slow crystallization of **12** took about two weeks.

In related complexes prepared from Ce^{3+} starting materials, O_2 reduction was associated with lanthanoid oxidation to the accessible +IV oxidation state.[108–112] Oxidation of Eu^{2+}, Sm^{2+}, and Nd^0 to the corresponding Ln^{3+} ions has also been reported as the electron source for O_2^{2-} formation.[107,113,114] Other works suggested organic ligands acting as sacrificial reducing agents to give the peroxide ion.[102,115] For **12**, it is possible that the autoxidation of thf[116,117] coupled with the reduction of O_2 produced the respective organic (hydro)peroxide whose breakdown led to the tetranuclear aggregate. Coordination of thf to the oxophilic gadolinium ions probably helped peroxidation, and the solvated Ln^{3+} species trapped the liberated O_2^{2-} as the thf hydroperoxide broke down. This mechanism has been shown to operate when the air autoxidation of 2-acetylpyridine in the presence of sodium picolinate and TbCl$_3$·6H$_2$O yielded the peroxide-bridged Tb^{3+} triangular complex [Tb$_3$(O$_2$)(pic)$_9$]$^{2-}$ (pic = picolinate, C$_5$H$_4$NCO$_2^-$).[98] Here again, complex **12** is unique – to the best of our knowledge, no other report of a similar reaction involving thf and lanthanoid ions has yet appeared in the literature.

Conclusion

The contribution of this work is threefold. In synthesis, we have shown that a large variety of anhydrous lanthanoid complexes can be obtained from a unifying and simple dehydration procedure. Products are accessible in high purity and yields, making this route very handy for reaching several starting materials. Second, and more surprising, although our current knowledge of the reactivity of rare-earth elements is much more extensive than when some of these compounds were first described, this chemistry still hides intriguing details, such as the formation mechanism of some unanticipated ligands (complex **11** as an example).

Several techniques have been employed to confirm the identity and purity of the products in bulk, and single-crystal X-ray diffraction was paramount to reveal compositional details. Additionally, thanks to our experimental and computational description of the relaxation dynamics of [DyCl$_3$(dme)$_2$] (compound **9**), we were able to discern between the two overlapping relaxation mechanisms, Raman and Orbach, at low and higher temperatures, respectively, an often trivialized attribution in the previous literature about lanthanide-based SIM, especially the ones featuring low relaxation barriers.

Experimental section

General

All manipulations were carried out under an inert atmosphere (N$_2$, 99.999%, Praxair or Air Liquide), using Schlenk and glovebox techniques. Solvents 1,2-dimethoxyethane (Aldrich), hexane (Vetec or Aldrich), and tetrahydrofuran (thf, Honeywell, or Aldrich) were purified and dried by standard methods[118] and distilled immediately before use. Propan-2-ol (Pr^{i}OH, Vetec, or Aldrich) was distilled first in the presence of calcium hydride (Aldrich) and then over sodium metal (Vetec or Riedel). Rare-earth salts, MCl$_3$·6H$_2$O (M = Y, Gd, Dy, Er, and Yb), and triethylorthoformate (teof), Acros Organics or Aldrich, were used without purification.

Instrumentation

Elemental analyses were performed under argon by MEDAC Laboratory (Chobham, Surrey, UK) on a Thermal Scientific Flash ES 1112 Series instrument. Fourier-transform infrared (FTIR) absorption spectra (4000 to 400 cm^{-1}) were recorded using BOMEN Michelson MB100 (4 cm^{-1} resolution) or BRUKER Vertex 70 (2 cm^{-1}) spectrophotometers. Samples were analyzed from emulsions in mineral oil (Nujol) previously dried with sodium metal.

Single-crystal X-ray diffraction data were collected on a Bruker D8 Venture diffractometer equipped with a Photon 100 CMOS detector and graphite monochromator. Mo-Kα radiation was used for all compounds. Due to their moisture sensitivity, the crystals were covered with mineral oil, mounted on a MicroMount™ support (MiTeGen), and cooled to 100 K (173 K

for product **5**) in the cold nitrogen stream before analysis. Data were processed using APEX2, APEX3, APEX4, or APEX5 software.[119–122] A face absorption correction (Gaussian from crystal shape)[123] was applied to complexes **2** and **6**, while a multi-scan absorption correction was employed for the other products.[120] Structures were determined by direct methods on SHELXS[124,125] or SHELXT,[126] and refined by full-matrix least-squares methods on F^2's in SHELXL.[127] All non-hydrogen atoms were refined with anisotropic thermal parameters. Hydrogen atoms not located in the difference maps were included in idealized positions, with their U_{iso} values set to ride on the U_{eq} values of the parent carbon atoms. Scattering factors for neutral atoms were taken from the literature. Complex **4** was treated as a two-component twin (BASF = 0.119 (2)). For complexes **6** and **8**, the PLATON analysis[128] did not indicate twinning, and the sizeable residual electron density peaks, far from the heavy atoms, suggested the presence of small additional crystallites during data collection. For complex **9**, in turn, although the observation of reflections very close to one another could explain the high electron density residuals far from the heavy atoms, PLATON analysis[128] did not provide a twin law, and it was not possible to solve for possible twinning. WinGX was used as a graphical interface to run the above software.[129] Structure drawings were made with the Diamond, ORTEP3, and Mercury programs.[130–132] The coordination geometries of the Ln^{3+} ions in complexes **1**, **2**, **9**, and **11** were confirmed from the crystallographic data using the SHAPE software.[133]

Powder X-ray diffractograms were recorded with Bruker D8 Discovery equipment using a high-brightness Cu-Kα X-ray microsource (*ca.* 50 μm) with a Montel multilayer focalization system (λ = 1.5406 Å). Samples were packed in Hilgenberg glass capillaries (0.5 mm diameter, glass no. 14) and measured with a rotating capillary Debye-Scherrer vertical setup at room temperature, employing 0.01° steps from 5° to 50° in 2θ. The measurement time was about 72 h for each sample. The powder patterns were analyzed with TOPAS v.5 software (Bruker AXS Corporation).[134]

^{1}H (400.13 MHz) and ^{13}C (100.03 MHz) NMR spectra were acquired at room temperature on a Bruker AVANCE 400 NMR spectrometer operating at 9.4 T and equipped with a 5 mm multinuclear direct detection probe. X-band EPR spectra (9.75 GHz) were obtained in the solid state at 300 and 77 K in a Bruker EMX Micro spectrometer. The crystalline samples were pulverized in the glovebox immediately before analysis.

The samples for magnetic characterization consisted of polycrystalline powders of products **6** and **9** wrapped in Teflon™ tape and pelletized to prevent magnetic orientation. The resulting data were corrected for the diamagnetic contributions of the samples, calculated from Pascal constants,[135] together with those measured for the sample holder and wrapping Teflon™ tape. The DC magnetic characterization was performed on a Quantum Design MPMS (Magnetic Properties Measurement System) platform with a 7 T magnet. The dependence of the magnetization (*M*) on the absolute temperature was investigated between 300 and 50 K using a magnetic field

(*B*) of 1 T and between 50 and 2 K with a field of 0.1 T to prevent magnetic saturation. The magnetic susceptibility per mole (χ_M) was then evaluated as $\chi_M = M_M/B$. AC susceptibilities were obtained for the same samples with a Physical Property Measurement System (PPMS; Quantum Design) in the frequency range of 10 to 10^4 Hz, with zero or 0.1 T applied static field. The recorded susceptibility data were fitted with the extended Debye method[88,89] to provide data on the relaxation time dependence on temperature.

Syntheses

The products **1**–**5** and **11**–**12** contain gadolinium(III), **6** and **9** contain dysprosium(III), **7**, **8**, and **10** contain yttrium(III), ytterbium(III), and erbium(III), respectively. Complexes **1**–**10** are the major products. Unanticipated **11** and **12** were formed accidentally in low yield.

Binuclear [Gd$_2$Cl$_4$(μ-Cl)$_2$(Pr^{i}OH)$_6$] (1). To a white suspension containing 1.60 g (4.30 mmol) of GdCl$_3$·6H$_2$O in 10.0 mL of isopropanol (Pr^{i}OH), 9.0 mL (54 mmol) of triethyl orthoformate (teof) were added. The mixture was stirred for 45 minutes at room temperature, forming a clear colorless solution. The solvent and excess teof were evaporated under vacuum, resulting in a white solid. This was dissolved in 30 mL of isopropanol, and the solution was again dried to remove the remaining alcohol and ester by-products. Finally, the white solid was dissolved in 25.0 mL of isopropanol, and the solution was cooled down to −20 °C. After 24 h, colorless block crystals of **1** were formed, which were soluble, at room temperature, in methanol, isopropanol, and thf, and insoluble in acetonitrile, dme, chloroform, hexane, and toluene. Solubilization in thf replaces the alcohol ligands, as described below (synthesis of complex **3**). Yield of **1**: 1.41 g, 74.0%. Elemental analysis (%) calcd for C$_{18}$H$_{48}$Cl$_6$Gd$_2$O$_6$: C 24.3, H 5.45; found: C 24.4, H 5.65.

Polymeric [{GdCl(μ-Cl)$_2$(thf)$_2$}$_\infty$] (2). The first step of this synthesis consists of the same dehydration process described for product **1**, this time starting from 1.15 g (3.09 mmol) of GdCl$_3$·6H$_2$O in Pr^{i}OH. The white solid obtained after drying the reaction mixture under vacuum was washed twice with hexane (2 × 15 mL), after which the solvent was evaporated to dryness. Tetrahydrofuran (10.0 mL) was added to the remaining product, stirred at room temperature, and evaporated under vacuum. Finally, 20.0 mL of thf were added to the resulting white solid, producing after mild heating (35 °C) a clear colorless solution that was cooled down to −20 °C. After 24 h, a microcrystalline white solid (0.91 g of **2**) was isolated by filtration. Recrystallization of this solid from a thf solution submitted to vapor diffusion of hexane produced colorless crystals suitable for X-ray diffraction analysis. The product was soluble in isopropanol, methanol, and hot tetrahydrofuran but insoluble in acetonitrile, dme, chloroform, hexane, and toluene. Yield: 0.91 g, 72.2% yield of [{GdCl(μ-Cl)$_2$(thf)$_2$}$_\infty$]. Elemental analysis (%) calcd for C$_8$H$_{16}$Cl$_3$GdO$_2$: C 23.6, H 3.95; found: C 23.5, H 4.04.

Mononuclear [GdCl$_3$(thf)$_4$] (3). 0.50 g (0.563 mmol) of **1**, [Gd$_2$Cl$_4$(μ-Cl)$_2$(Pr^{i}OH)$_6$], was dissolved in 30.0 mL of thf, producing a colorless solution that was stirred at room tempera-

ture for 20 minutes. The solvent was then removed under vacuum, giving a white solid that was redissolved in 30.0 mL of thf. Crystallization occurred by vapor diffusion of hexane into this thf solution in the glove box. After five days, colorless crystals were isolated, washed with hexane, and dried under vacuum. The product is soluble in isopropanol, methanol, and hot tetrahydrofuran. Yield: 0.59 g (95.1%). Elemental analysis (%) calcd for $C_{16}H_{32}Cl_3GdO_4$: C 34.8, H 5.84; found: C 32.1, H 5.68%. A formulation consistent with the elemental analysis results considers the loss of 0.6 mol of thf per mol of product, $C_{13.6}H_{27.2}Cl_3GdO_{3.4}$, which gives C_{calc} = 32.1%, H_{calc} = 5.40%. Several batches of crystals of **3** were obtained during this work, and, in all cases, single-crystal X-ray diffraction analysis confirmed the product's identity.

***trans*-[GdCl₂(thf)₅]*trans*-[GdCl₄(thf)₂]** (4). Triethylorthoformate (5.4 mL, 33.0 mmol) was added to a suspension of GdCl₃·6H₂O (1.01 g, 2.72 mmol) in 7.0 mL of thf. After stirring for 40 min at room temperature, a clear colorless solution was obtained, from which the solvent, excess teof, and reaction by-products were removed under vacuum. The remaining white solid was suspended in 30 mL of thf, dissolving completely after stirring at 50 °C for 30 min. Small colorless crystals formed as this solution was left to cool down and then kept at room temperature for 24 hours. The crystalline product was filtered and dried under N₂ flow to reduce solvent loss compared to drying under vacuum. The crystals were soluble in isopropanol and tetrahydrofuran but insoluble in acetonitrile, dme, chloroform, hexane, and toluene. Yield: 0.87 g, 62.1% yield. Elemental analysis (%) calcd for $C_{28}H_{56}Cl_6Gd_2O_7$: C 32.6, H 5.47; found C 32.1, H 5.68.

Mononuclear [GdCl₃(dme)₂] (5). To a solution containing 0.44 g (1.40 mmol) of product **1**, [Gd₂Cl₄(μ-Cl)₂(Pr^{i}OH)₆], in 5.0 mL of Pr^{i}OH, 10 mL of dme were slowly and carefully added, forming a biphasic system. After complete liquid diffusion (*ca.* three days), small block-shaped crystals were filtered and dried under vacuum. Crystals were soluble in methanol, isopropanol, and thf and insoluble in acetonitrile, dme, chloroform, hexane, and toluene. Yield: 0.33 g (75.0%). Elemental analysis (%) calcd for $C_8H_{20}Cl_3GdO_4$: C 21.6, H 4.54; found: C 21.6, H 4.79.

This complex was also prepared directly from GdCl₃·6H₂O (1.26 g, 3.39 mmol) in dme (30 mL) upon the addition of 8.0 mL (48 mmol) of teof. The white suspension soon turned into a colorless solution that was left stirring under reflux for 2 h. After solvent evaporation to dryness, the remaining white solid was suspended in dme to receive a new addition (8.0 mL) of teof. This time, however, only a portion of the solid dissolved. This reaction mixture was filtered, and the filtrate was cooled to −20 °C. After six days, colorless crystals of **5** (0.238 g, 15% yield) were isolated and dried under vacuum. Single-crystal XRD confirmed the product's identity (CCDC deposition number 2403176†). This route was not optimized; the low yield probably comes from the low solubility of the product in the second dehydration step.

***trans*-[DyCl₂(thf)₅]*trans*-[DyCl₄(thf)₂] (6).** The synthesis was similar to that of the Gd analog **4**, starting from 1.03 g

(2.73 mmol) of DyCl₃·6H₂O and 5.5 mL (33.0 mmol) of teof in 7.0 mL of thf. Following the complete workup, including heating the reaction mixture at 75 °C for 15 min, colorless crystals formed from the thf mother liquor after 1 h at −20 °C. They were then filtered and dried under dinitrogen flow. Their solubility was like the reported for product **4**. Yield: 1.04 g, 73.2% yield. Elemental analysis (%) calcd for $C_{28}H_{56}Cl_6Dy_2O_7$: C 32.3, H 5.41; found: C 30.2, H 5.85. Carbon content is low but compatible with the literature.[75] Considering the loss of one thf molecule, which would lead to the formulation $C_{24}H_{48}Cl_6O_6Dy_2$, the calculated (%) contents of C 29.7, and H 4.99, are close to the experimental figures. The identity and purity of the product in the bulk were confirmed by powder X-ray diffraction analysis (see ESI, Fig. S6†).

***trans*-[YCl₂(thf)₅]*trans*-[YCl₄(thf)₂] (7).** To a suspension containing 2.49 g (8.21 mmol) of YCl₃·6H₂O in 40.0 mL of thf, 17.1 mL (102.6 mmol) of triethyl orthoformate (teof) were added, producing a colorless solution. After overnight stirring at room temperature, the solvent, excess teof, and by-products of teof hydrolysis were removed under vacuum with slight heating. The remaining white solid received the addition of thf (40 mL) and was left stirring overnight. There was no complete dissolution, so the system was heated under reflux at 80 °C for 2 h. The remaining thin suspension was then filtered through Celite while hot, and the resulting filtrate was cooled to −20 °C for two days, during which a microcrystalline solid formed. It was then filtered off and dried under N₂ flow to avoid losing coordinating thf, as the crystals become opaque when dried under vacuum. The product was soluble in isopropanol, insoluble in hexane, and partially soluble in thf at room temperature. In the case of thf, mild heating at *ca.* 50 °C ensures total solubilization. Yield: 4.48 g (6.24 mmol, 76.0%). The product's identity in the bulk was confirmed by powder X-ray diffraction analysis (Fig. S5†).

Mononuclear [YbCl₃(thf)₃] (8). To a suspension of 1.02 g (3.17 mmol) of YbCl₃·6H₂O in 30.0 mL of thf, 6.60 mL (39.7 mmol) of teof were added. The system was stirred at room temperature for twenty minutes, giving a colorless solution. After solvent (and by-products) removal by vacuum, the white product was treated again with thf (30.0 mL) and teof (6.60 mL). The resulting suspension was stirred overnight at room temperature, filtered through Celite to remove a small amount of solid, and cooled to −20 °C. Colorless crystals were isolated by filtration and dried under N₂ flow. Their solubility was like the reported for product **7**. Yield: 1.33 g, 85.0%. The identity and purity of the mononuclear product in the bulk were confirmed by powder X-ray diffraction analysis (Fig. S5†).

Mononuclear [DyCl₃(dme)₂] (9). This procedure resembles the described above for **5**, only starting directly from the commercial (hydrated) salt instead of first preparing the isopropanol solvate. To a suspension containing 0.53 g (1.40 mmol) of DyCl₃·6H₂O in 3.4 mL of Pr^{i}OH, 3.0 mL (18.0 mmol) of teof were added. The system was kept under magnetic stirring for 20 minutes, after which the liquid phase was removed under vacuum, giving a pale yellowish solid. This was dissolved in 10.0 mL of Pr^{i}OH, and, to the resulting solution, 15.0 mL of

dme were slowly and carefully added. After three days, block-shaped crystals were isolated by filtration and dried under vacuum. Solubility was like that of product **5**. Yield: 0.43 g, 68.0%. Elemental analysis (%) calcd for $C_8H_{20}Cl_3DyO_4$: C 21.4, H 4.49; found: C 21.1, H 4.95.

Mononuclear [ErCl₃(dme)₂] (10). In a Schlenk flask, 2.74 mmol (1.04 g) of erbium(III) chloride hexahydrate was suspended in 40 mL of dme, and to this suspension, 5.50 mL (32.85 mmol) of triethylorthoformate were added. The erbium salt did not dissolve, even after stirring for 12 hours. Subsequently, the solvent and triethylorthoformate residues were removed under vacuum, resulting in a light pink solid. The addition of dme and triethylorthoformate (same quantities above) was repeated, but no dissolution occurred. The mixture was refluxed at 85 °C for 2 hours, leading to solubilization. After filtration through Celite, the resulting pink solution was cooled to −20 °C, forming 0.756 g of light pink crystals (76% yield). The solubility of **10** resembles that of **5**. Elemental analysis (%) calcd for $C_8H_{20}Cl_3ErO_4$: C 21.2, H 4.44; found: C 21.1, H 4.93.

Polymeric [({Gd₃Cl₄(μ-Cl)₄(μ-H₃CCOO)(C₃H₈O₂) (Pr^iOH)₄}·Pr^iOH)∞] (11). A mixture of gadolinium(III) chloride hexahydrate (1.02 g, 2.74 mmol), isopropanol (7.30 mL, 95.6 mmol), and triethyl orthoformate (16.0 mL, 96.1 mmol) produced a clear, colorless solution upon stirring for 15 min at room temperature. After an additional 30 min, the solvent was completely removed under vacuum, resulting in a white solid. This procedure (addition of Pr^iOH and a large excess of teof, followed by complete evaporation of the solvent and liquid products) was repeated twice more. The final white solid (product **A**, 1.35 g) was then washed with hexane (2 × 15.0 mL), filtered, and dried under vacuum. Product **A** was soluble in methanol, isopropanol, and tetrahydrofuran and insoluble or partially soluble in toluene, dme, and hexane. For recrystallization, 120 mg of **A** were dissolved in 7.0 mL of Pr^iOH and submitted to vapor diffusion of dimethoxyethane (25.0 mL) in the glovebox for four days. After this period, as there was no crystallization, the clear solution was cooled down to −20 °C for one week, after which, still with no crystallization, it was submitted again to vapor diffusion, this time with hexane, in the glove box, where it was kept for one more week. Again, there were no crystals or precipitation, so this procedure (cooling to −20 °C and vapor diffusion with hexane) was repeated. Finally, colorless crystals of the polymeric complex **11** were obtained and isolated after one more week. Yield: 25 mg, 23.4% yield based on Gd. Elemental analysis (%) calcd for $C_{17}H_{43}Cl_8Gd_3O_8·C_3H_8O$ (product **11**): C 20.2, H 4.32; found for product **A**: C 19.2, H 4.46. This result suggests partial loss of the solvating isopropanol.

Tetranuclear [{(thf)₂Cl₂Gd(μ-Cl)₂(μ₃-O₂)Gd(thf)₃}₂]·3thf (12). In a repetition of the synthesis of complex **2**, the mother liquor recovered after the isolation of the white microcrystalline product (**2**) was cooled down again to −20 °C. After 13 days, *ca.* 20 mg of colorless block crystals of **12** were formed, which became powdery after solvent removal. Single-crystal X-ray data was collected at 100(2) K from a crystal quickly taken directly from the mother solution to prevent decomposition. The small amount of product and its difficult manipulation prevented full characterization.

Computational methods

The calculations on compound **9** were performed on X-ray crystal structure coordinates without further geometry optimizations. All simulations were performed using ORCA 5.0.2 Quantum Chemistry Software Package.[136] Second-order Douglas–Kroll–Hess Hamiltonian has been employed to consider scalar relativistic corrections. SARC2-QZVP basis sets[137] were employed for the lanthanide ion, while DKH-def2-TZVP[138] was used for all other atomic species. The resolution of identity (RI) approximation was applied with the default settings for the integration grids,[138] and the AUTOAUX feature was used to generate the corresponding auxiliary basis sets automatically. The energy ladder of the electronic states for the lanthanide ion has been computed using the CASSCF method, followed by Spin–Orbit coupling calculations within the Quasi-Degenerate Perturbation Theory (QDPT) and mean field approaches. The chosen active space for the lanthanides consisted of the nine unpaired electrons in the seven 4f orbitals of the Dy^{3+} ion, CAS (9,7). Due to hardware limitations, only the states with the highest spin multiplicity, 21 sextuplets for Dy, were computed and included in the subsequent spin–orbit calculation. The g-tensor and the Extended Stevens' Operator (ESO) were calculated using the SINGLE_ANISO module[139,140] implemented in ORCA.

Author contributions

ology, project administration, resources, supervision, validation, writing – original draft, writing – review & editing.

Data availability

The data supporting this article can be found in the main text and the ESI† or are available from the authors upon reasonable request. Tables S1–S17† and plots Fig. S1–S18† of crystallographic, structural, spectroscopic (FTIR, NMR, EPR), and magnetic susceptibility data and details of theoretical calculations are supplied as a PDF file.

Conflicts of interest

There are no conflicts of interest to declare.

Acknowledgements

References

1 J.-C. G. Bünzli, *Acc. Chem. Res.*, 2006, **39**, 53–61.
2 T. Behrsing, V. L. Blair, F. Jaroschik, G. B. Deacon and P. C. Junk, *Molecules*, 2024, **29**, 688.
3 B. Zheng, J. Fan, B. Chen, X. Qin, J. Wang, F. Wang, R. Deng and X. Liu, *Chem. Rev.*, 2022, **122**, 5519–5603.
4 K. Du, J. Feng, X. Gao and H. Zhang, *Light: Sci. Appl.*, 2022, **11**, 222.
5 Q. Wu, Q. Zheng, Y. He, Q. Chen and H. Yang, *Anal. Chem.*, 2023, **95**, 33–48.
6 N. Iyad, M. S. Ahmad, S. G. Alkhatib and M. Hjouj, *Eur. J. Radiol. Open*, 2023, **11**, 100503.
7 M. J. Bai, H. Wan, Y. Zhang, S. Q. Chen, C. Y. Lu, X. H. Liu, G. Chen, N. Zhang and R. Z. Ma, *Chem. Sci.*, 2024, **15**, 16887–16907.
8 P. Li and H. Li, *Coord. Chem. Rev.*, 2021, **441**, 213988.
9 P. Singh, S. Kachhap, P. Singh and S. K. Singh, *Coord. Chem. Rev.*, 2022, **472**, 214795.
10 J. Hayashi, S. Shoji, Y. Kitagawa and Y. Hasegawa, *Coord. Chem. Rev.*, 2022, **467**, 214607.
11 A. G. Bispo Jr., N. A. Oliveira, I. M. S. Diogenis and F. A. Sigoli, *Coord. Chem. Rev.*, 2025, **523**, 216279.
12 C. Pagis, M. Ferbinteanu, G. Rothenberg and S. Tanase, *ACS Catal.*, 2016, **6**, 6063–6072.
13 Z. Liang, L. Yin, H. Yin, Z. Yin and Y. Du, *Nanoscale Horiz.*, 2022, **7**, 31–40.
14 M. K. Hossain, M. H. K. Rubel, M. A. Akbar, M. H. Ahmed, N. Haque, M. F. Rahman, J. Hossain and K. M. Hossain, *Ceram. Int.*, 2022, **48**, 32588–32612.
15 L. Li, T. Zhang, Y. Zhou, X. Wang, C.-T. Au and L. Jiang, *J. Rare Earths*, 2022, **40**, 1–10.
16 F. Adams, *Macromol. Rapid Commun.*, 2024, **45**, 2400122.
17 L.-X. You, B.-Y. Ren, Y.-K. He, S.-J. Wang, Y.-G. Sun, V. Dragutan, G. Xiong and F. Ding, *J. Mol. Struct.*, 2024, **1304**, 137687.
18 K. Bernot, *Eur. J. Inorg. Chem.*, 2023, **26**, e202300336.
19 V. Vieru, S. Gómez-Coca, E. Ruiz and L. F. Chibotaru, *Angew. Chem., Int. Ed.*, 2024, **63**, e202303146.
20 J. T. Li, J. Yang, Q. Q. Yu, G. R. Su and W. Liu, *J. Phys. Chem. C*, 2024, **128**, 4882–4890.
21 I. Ahmad, S. Shukrullah, M. Y. Naz, H. N. Bhatti, M. Ahmad, E. Ahmed, S. Ullah and M. Hussien, *J. Environ. Chem. Eng.*, 2022, **10**, 107762.
22 Q. Wang, H. Fan, Y. Xiao and Y. Zhang, *J. Rare Earths*, 2022, **40**, 1668–1681.
23 M. K. Hossain, G. A. Raihan, M. A. Akbar, M. H. Kabir Rubel, M. H. Ahmed, M. I. Khan, S. Hossain, S. K. Sen, M. I. E. Jalal and A. El-Denglawey, *ACS Appl. Electron. Mater.*, 2022, **4**, 3327–3353.
24 Y. U. Li, K. Wang, X. M. Wang, Z. J. Wang, J. Xu, M. Zhao, X. Wang, S. Y. Song and H. J. Zhang, *Chin. J. Catal.*, 2024, **61**, 54–70.
25 F. Ortu, *Chem. Rev.*, 2022, **122**, 6040–6116.
26 M. D. Taylor, *Chem. Rev.*, 1962, **62**, 503–511.
27 J. Burgess and J. Kijowski, in *Advances in Inorganic Chemistry and Radiochemistry*, ed. H. J. Emeléus and A. G. Sharpe, Academic Press, 1981, vol. 24, pp. 57–114.
28 F. L. Carter and J. F. Murray, *Mater. Res. Bull.*, 1972, **7**, 519–523.
29 G. B. Deacon, T. D. Tuong, D. L. Wilkinson and T. Marks, in *Inorg. Synth*, 1990, pp. 286–291. DOI: 10.1002/9780470132593.ch72.
30 J. B. Reed, B. S. Hopkins and L. F. Audrieth, *J. Am. Chem. Soc.*, 1935, **57**, 1159–1160.
31 G. Meyer, E. Garcia and J. D. Corbett, in *Inorg. Synth*, 1989, pp. 146–150. DOI: 10.1002/9780470132562.ch35.
32 M. Simon and G. Meyer, *Z. Kristallogr. - Cryst. Mater.*, 1996, **211**, 327–327.
33 G. Meyer, N. Cesur and I. Pantenburg, *Acta Crystallogr., Sect. E: Struct. Rep. Online*, 2003, **59**, i145–i146.

34 N. L. Edleman, A. Wang, J. A. Belot, A. W. Metz, J. R. Babcock, A. M. Kawaoka, J. Ni, M. V. Metz, C. J. Flaschenriem, C. L. Stern, L. M. Liable-Sands, A. L. Rheingold, P. R. Markworth, R. P. H. Chang, M. P. Chudzik, C. R. Kannewurf and T. J. Marks, *Inorg. Chem.*, 2002, **41**, 5005–5023.

35 S. Mishra, *Coord. Chem. Rev.*, 2008, **252**, 1996–2025.

36 A. Drozdov and N. Kuzmina, in *Comprehensive Inorganic Chemistry II*, ed. J. Reedijk and K. Poeppelmeier, Elsevier, Amsterdam, 2nd edn, 2013, pp. 511–534. DOI: 10.1016/B978-0-08-097774-4.00223-0.

37 R. G. Bulgakov, S. P. Kuleshov, A. N. Zuzlov, I. R. Mullagaleev, L. M. Khalilov and U. M. Dzhemilev, *J. Organomet. Chem.*, 2001, **636**, 56–62.

38 N. Mahé, O. Guillou, C. Daiguebonne, Y. Gérault, A. Caneschi, C. Sangregorio, J. Y. Chane-Ching, P. E. Car and T. Roisnel, *Inorg. Chem.*, 2005, **44**, 7743–7750.

39 J. H. Freeman and M. L. Smith, *J. Inorg. Nucl. Chem.*, 1958, **7**, 224–227.

40 D. D. Wirth, S. Vikas and P. Jagadish, in *Encyclopedia of Reagents for Organic Synthesis*, 2017, pp. 1–6. DOI: 10.1002/047084289X.rt099.pub2.

41 E. M. Khalaf, M. J. Mohammadi, S. Sulistiyani, A. A. Ramírez-Coronel, F. Kiani, A. T. Jalil, A. F. Almulla, P. Asban, M. Farhadi and M. Derikondi, *Rev. Environ. Health*, 2024, **39**, 331–337.

42 P. Di Bernardo, A. Melchior, M. Tolazzi and P. L. Zanonato, *Coord. Chem. Rev.*, 2012, **256**, 328–351.

43 U. Baisch, D. B. DellAmico, F. Calderazzo, R. Conti, L. Labella, F. Marchetti and E. A. Quadrelli, *Inorg. Chim. Acta*, 2004, **357**, 1538–1548.

44 G. B. Deacon and A. J. Koplick, *Inorg. Nucl. Chem. Lett.*, 1979, **15**, 263–265.

45 S.-H. Wu, Z.-B. Ding and X.-J. Li, *Polyhedron*, 1994, **13**, 2679–2681.

46 S. Petriček, *Acta Chim. Slov.*, 2009, **56**, 426–433.

47 G. B. Deacon, T. Feng, S. Nickel, B. W. Skelton and A. H. White, *J. Chem. Soc., Chem. Commun.*, 1993, 1328–1329, DOI: 10.1039/C39930001328.

48 G. B. Deacon, T. Feng, P. C. Junk, B. W. Skelton, A. N. Sobolev and A. H. White, *Aust. J. Chem.*, 1998, **51**, 75–89.

49 G. B. Deacon, T. Feng, P. C. Junk, G. Meyer, N. M. Scott, B. W. Skelton and A. H. White, *Aust. J. Chem.*, 2001, **53**, 853–865.

50 C. T. Carver, M. J. Monreal and P. L. Diaconescu, *Organometallics*, 2008, **27**, 363–370.

51 W. Huang, B. M. Upton, S. I. Khan and P. L. Diaconescu, *Organometallics*, 2013, **32**, 1379–1386.

52 W. Huang, J. L. Brosmer and P. L. Diaconescu, *New J. Chem.*, 2015, **39**, 7696–7702.

53 D. M. Barnhart, T. M. Frankcom, P. L. Gordon, N. N. Sauer, J. A. Thompson and J. G. Watkin, *Inorg. Chem.*, 1995, **34**, 4862–4867.

54 K. Izod, S. T. Liddle and W. Clegg, *Inorg. Chem.*, 2004, **43**, 214–218.

55 G. R. Giesbrecht, J. C. Gordon, D. L. Clark and B. L. Scott, *Inorg. Chem.*, 2004, **43**, 1065–1070.

56 G. R. Willey, T. J. Woodman and M. G. B. Drew, *Polyhedron*, 1997, **16**, 3385–3393.

57 Z. Khademi and K. Nikoofar, *RSC Adv.*, 2020, **10**, 30314–30397.

58 Z. Nazarian and M. Dabiri, *ChemistrySelect*, 2020, **5**, 4394–4412.

59 G. G. Nunes, R. C. R. Bottini, D. M. Reis, P. H. C. Camargo, D. J. Evans, P. B. Hitchcock, G. Jeffery Leigh, E. L. Sá and J. F. Soares, *Inorg. Chim. Acta*, 2004, **357**, 1219–1228.

60 A. R. Hilts and J. Cooke, *J. Chem. Educ.*, 2023, **100**, 4119–4121.

61 S. Hollstein and M. von Delius, *Acc. Chem. Res.*, 2024, **57**, 602–612.

62 A. Merbach, M.-N. Pitteloud and P. Jaccard, *Helv. Chim. Acta*, 1972, **55**, 44–52.

63 M. Niemeyer, *Z. Anorg. Allg. Chem.*, 2006, **632**, 1449–1456.

64 J.-R. Li, R.-H. Zhang and X.-H. Bu, *Eur. J. Inorg. Chem.*, 2005, **2005**, 1913–1918.

65 M. Seitz, A. G. Oliver and K. N. Raymond, *J. Am. Chem. Soc.*, 2007, **129**, 11153–11160.

66 C. Krupczak, B. J. Stoeberl, K. C. M. Westrup, L. Tesi, F. S. Santana, S. O. K. Giese, F. Yokaichiya, D. d. S. Costa, J. M. Missina, D. Stinghen, D. L. Hughes, R. Sessoli, G. G. Nunes, D. M. Reis and J. F. Soares, *J. Mol. Struct.*, 2023, **1274**, 134360.

67 D. L. Clark, J. C. Gordon, B. L. Scott and J. G. Watkin, *Polyhedron*, 1999, **18**, 1389–1396.

68 D. M. Pajerowski, Q. Li, J. Hyun, C. L. Dennis, D. Phelan, P. Yan, P. Chen and G. Li, *Dalton Trans.*, 2014, **43**, 11973–11980.

69 S. Mathur, H. Shen, N. Lecerf, A. Kjekshus, H. Fjellvåg and G. F. Goya, *Adv. Mater.*, 2002, **14**, 1405–1409.

70 A. I. Yanovsky, Z. A. Starikova, E. P. Turevskaya, N. Y. Turova, A. P. Pisarevsky and Y. T. Struchkov, *Zh. Neorg. Khim.*, 1996, **41**, 1248–1254.

71 M. Schäfer and R. Herbst-Irmer, *Acta Crystallogr., Sect. C: Cryst. Struct. Commun.*, 1994, **50**, 1256–1258.

72 S. A. Vaughn, R. C. Severance, M. D. Smith and H.-C. Z. Loye, *Solid State Sci.*, 2012, **14**, 1343–1348.

73 J. Zhongsheng, W. Shenglong and W. Fusong, *Chem. J. Chin. Univ.*, 1985, **6**, 735–737.

74 W. J. Evans, J. L. Shreeve, J. W. Ziller and R. Doedens, *Inorg. Chem.*, 1995, **52**, 576–585.

75 G. R. Willey, P. R. Meehan, T. J. Woodman and M. G. B. Drew, *Polyhedron*, 1997, **16**, 623–627.

76 P. Sobota, J. Utko and S. Szafert, *Inorg. Chem.*, 1994, **33**, 5203–5206.

77 S. Anfang, M. Karl, N. Faza, W. Massa, K. Magull and K. Dehnicke, *Z. Anorg. Allg. Chem.*, 1997, **623**, 1425–1432.

78 R. D. Shannon, *Acta Crystallogr., Sect. A*, 1976, **32**, 751–767.

79 *CRC Handbook of Chemistry and Physics*, ed. W. M. Haynes, CRC Press, Boca Raton, 95th edn, 2014.

80 D. B. Dell'Amico, F. Calderazzo, C. della Porta, A. Merigo, P. Biagini, G. Lugli and T. Wagner, *Inorg. Chim. Acta*, 1995, **240**, 1–3.

81 S. Anfang, K. Dehnicke and J. Magull, *Z. Naturforsch., B: Chem. Sci.*, 1996, **51**, 531–535.

82 L. Sorace and D. Gatteschi, in *Lanthanides and Actinides in Molecular Magnetism*, 2015, pp. 1–26. DOI: 10.1002/9783527673476.ch1.

83 J. M. Clemente-Juan, E. Coronado and A. Gaita-Ariño, in *Lanthanides and Actinides in Molecular Magnetism*, 2015, pp. 27–60. DOI: 10.1002/9783527673476.ch2.

84 J. D. Rinehart and J. R. Long, *Chem. Sci.*, 2011, **2**, 2078–2085.

85 C. A. Goodwin, F. Ortu, D. Reta, N. F. Chilton and D. P. Mills, *Nature*, 2017, **548**, 439–442.

86 J.-L. Liu, Y.-C. Chen and M.-L. Tong, *Chem. Soc. Rev.*, 2018, **47**, 2431–2453.

87 K. L. M. Harriman, D. Errulat and M. Murugesu, *Trends Chem.*, 2019, **1**, 425–439.

88 K. S. Cole and R. H. Cole, *J. Chem. Phys.*, 1941, **9**, 341–351.

89 C. Dekker, A. F. M. Arts, H. W. de Wijn, A. J. van Duyneveldt and J. A. Mydosh, *Phys. Rev. B: Condens. Matter Mater. Phys.*, 1989, **40**, 11243–11251.

90 L. Tesi, A. Lunghi, M. Atzori, E. Lucaccini, L. Sorace, F. Totti and R. Sessoli, *Dalton Trans.*, 2016, **45**, 16635–16643.

91 R. N. Soek, C. M. Ferreira, F. S. Santana, D. L. Hughes, G. Poneti, R. R. Ribeiro and F. S. Nunes, *J. Mol. Struct.*, 2019, **1184**, 254–261.

92 S. Mondal and A. Lunghi, *J. Am. Chem. Soc.*, 2022, **144**, 22965–22975.

93 A. Lunghi, F. Totti, R. Sessoli and S. Sanvito, *Nat. Commun.*, 2017, **8**, 14620.

94 E. Lucaccini, L. Sorace, M. Perfetti, J.-P. Costes and R. Sessoli, *Chem. Commun.*, 2014, **50**, 1648–1651.

95 F. Marchetti, G. Pampaloni and S. Zacchini, *Dalton Trans.*, 2008, 7026–7035, DOI: 10.1039/B810210D.

96 R. Bini, F. Marchetti, G. Pampaloni and S. Zacchini, *Polyhedron*, 2011, **30**, 1412–1419.

97 P. Che, F. Lu, X. Si and J. Xu, *RSC Adv.*, 2015, **5**, 24139–24143.

98 W. J. Gee, J. G. MacLellan, C. M. Forsyth, B. Moubaraki, K. S. Murray, P. C. Andrews and P. C. Junk, *Inorg. Chem.*, 2012, **51**, 8661–8663.

99 P. W. Roesky, G. Canseco-Melchor and A. Zulys, *Chem. Commun.*, 2004, 738–739, DOI: 10.1039/B315218A.

100 P. C. Andrews, T. Beck, C. M. Forsyth, B. H. Fraser, P. C. Junk, M. Massi and P. W. Roesky, *Dalton Trans.*, 2007, 5651–5654, DOI: 10.1039/B710534G.

101 J. T. Miller, Y. Ren, S. Li, K. Tan, G. McCandless, C. Jacob, Z. Wu, C.-W. Chu, B. Lv, M. C. Biewer and M. C. Stefan, *Inorg. Chem.*, 2020, **59**, 10379–10383.

102 B. Neumüller, F. Weller, T. Gröb and K. Dehnicke, *Z. Anorg. Allg. Chem.*, 2002, **628**, 2365–2371.

103 X.-T. Wang, H.-M. Dong, X.-G. Wang, E.-C. Yang and X.-J. Zhao, *Z. Anorg. Allg. Chem.*, 2016, **642**, 1166–1172.

104 H. Ke, X. Lu, W. Wei, W. Wang, G. Xie and S. Chen, *Dalton Trans.*, 2017, **46**, 8138–8145.

105 C.-M. Liu, D.-Q. Zhang, X. Hao and D.-B. Zhu, *Inorg. Chem. Front.*, 2020, **7**, 3340–3351.

106 P. Kumar, J. Flores Gonzalez, P. P. Sahu, N. Ahmed, J. Acharya, V. Kumar, O. Cador, F. Pointillart, S. K. Singh and V. Chandrasekhar, *Inorg. Chem. Front.*, 2022, **9**, 5072–5092.

107 G. B. Deacon, C. M. Forsyth, D. Freckmann, P. C. Junk, K. Konstas, J. Luu, G. Meyer and D. Werner, *Aust. J. Chem.*, 2014, **67**, 1860–1865.

108 A. Mustapha, J. Reglinski and A. R. Kennedy, *Inorg. Chim. Acta*, 2009, **362**, 1267–1274.

109 M. P. Coles, P. B. Hitchcock, A. V. Khvostov, M. F. Lappert, Z. Li and A. V. Protchenko, *Dalton Trans.*, 2010, **39**, 6780–6788.

110 Y.-L. Sang, X.-S. Lin, X.-C. Li, Y.-H. Liu and X.-H. Zhang, *Inorg. Chem. Commun.*, 2015, **62**, 115–118.

111 M. Paul, S. Shirase, Y. Morimoto, L. Mathey, B. Murugesapandian, S. Tanaka, S. Itoh, H. Tsurugi and K. Mashima, *Chem. – Eur. J.*, 2016, **22**, 4008–4014.

112 S. Shirase, K. Shinohara, H. Tsurugi and K. Mashima, *ACS Catal.*, 2018, **8**, 6939–6947.

113 M. Xémard, V. Goudy, A. Braun, M. Tricoire, M. Cordier, L. Ricard, L. Castro, E. Louyriac, C. E. Kefalidis, C. Clavaguéra, L. Maron and G. Nocton, *Organometallics*, 2017, **36**, 4660–4668.

114 N. J. C. van Velzen and S. Harder, *Organometallics*, 2018, **37**, 2263–2271.

115 D. M. Roitershtein, A. A. Vinogradov, K. A. Lyssenko and I. E. Nifant'ev, *Inorg. Chem. Commun.*, 2017, **84**, 225–228.

116 A. Robertson and W. A. Waters, *Trans. Faraday Soc.*, 1946, **42**, 201–210.

117 H. Matsubara, S. Suzuki and S. Hirano, *Org. Biomol. Chem.*, 2015, **13**, 4686–4692.

118 D. D. Perrin and W. L. Armarego, *Purification of Laboratory Chemicals*, Butterworth-Heinemann, Oxford, 3rd edn, 1997.

119 *APEX2 software*, Bruker AXS, Madison, Wisconsin, USA, 2014.

120 *APEX3, SAINT and SADABS software*, Bruker AXS Inc., Madison, Wisconsin, USA, 2016.

121 *APEX4, SAINT and SADABS software*, Bruker AXS Inc., Madison, Wisconsin, USA, 2021.

122 *APEX5 software*, Bruker AXS Inc., Madison, Wisconsin, USA, 2023.

123 P. Coppens, L. Leiserowitz and D. Rabinovich, *Acta Crystallogr.*, 1965, **18**, 1035–1038.

124 G. Sheldrick, *Acta Crystallogr., Sect. A: Found. Adv.*, 2008, **64**, 112–122.

125 G. M. Sheldrick, *SHELXS – Programs for crystal structure determination (SHELXS-2013)*, University of Göttingen, Germany, 2013.

126 G. M. Sheldrick, *Acta Crystallogr., Sect. A: Found. Adv.*, 2015, **71**, 3–8.

127 G. M. Sheldrick, *Acta Crystallogr., Sect. C: Struct. Chem.*, 2015, **71**, 3–8.

128 A. L. Spek, *Acta Crystallogr., Sect. D: Biol. Crystallogr.*, 2009, **65**, 148–155.

129 L. J. Farrugia, *J. Appl. Crystallogr.*, 2012, **45**, 849–854.

130 L. J. Farrugia, *J. Appl. Crystallogr.*, 1997, **30**, 565–565.

131 K. Brandenburg, *DIAMOND software*, Crystal Impact GbR, Bonn, Germany, 2006.

132 C. F. Macrae, I. Sovago, S. J. Cottrell, P. T. Galek, P. McCabe, E. Pidcock, M. Platings, G. P. Shields, J. S. Stevens and M. Towler, *J. Appl. Crystallogr.*, 2020, **53**, 226–235.

133 M. Llunell, D. Casanova, J. Cirera, J. Bofill, P. Alemany, S. Alvarez, M. Pinsky and D. Avnir, *Program for the Stereochemical Analysis of Molecular Fragments by Means of Continuous Shape Measures and Associated Tools*, University of Barcelona, Barcelona, Spain, 2005.

134 A. A. Coelho, *J. Appl. Crystallogr.*, 2018, **51**, 210–218.

135 G. A. Bain and J. F. Berry, *J. Chem. Educ.*, 2008, **85**, 532–536.

136 F. Neese, F. Wennmohs, U. Becker and C. Riplinger, *J. Chem. Phys.*, 2020, **152**, 224108.

137 D. Aravena, F. Neese and D. A. Pantazis, *J. Chem. Theory Comput.*, 2016, **12**, 1148–1156.

138 F. Weigend and R. Ahlrichs, *Phys. Chem. Chem. Phys.*, 2005, **7**, 3297–3305.

139 L. F. Chibotaru and L. Ungur, *J. Chem. Phys.*, 2012, **137**, 064112.

140 L. Ungur and L. F. Chibotaru, *Chem. – Eur. J.*, 2017, **23**, 3708–3718.